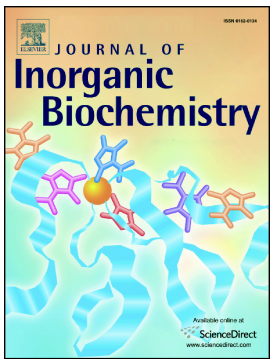

Cu(II) coordination to His-containing linear peptides and related branched ones: Equalities and diversities

Monica Perinelli, Remo Guerrini, Valentina Albanese, Nicola Marchetti, Denise Bellotti, Silvia Gentili, Matteo Tegoni, Maurizio Remelli

PII: S0162-0134(19)30639-7

DOI: https://doi.org/10.1016/j.jinorgbio.2019.110980

Reference: JIB 110980

To appear in: *Journal of Inorganic Biochemistry*

Received date: 1 October 2019

Revised date: 13 December 2019

Accepted date: 24 December 2019

Please cite this article as: M. Perinelli, R. Guerrini, V. Albanese, et al., Cu(II) coordination to His-containing linear peptides and related branched ones: Equalities and diversities, *Journal of Inorganic Biochemistry* (2018), https://doi.org/10.1016/j.jinorgbio.2019.110980

Cu(II) coordination to His-containing linear peptides and related branched ones: equalities and diversities

Monica Perinelli,[a,#] Remo Guerrini,[b] Valentina Albanese,[b] Nicola Marchetti,[b] Denise Bellotti,[b] Silvia Gentili,[a] Matteo Tegoni,[a,*] Maurizio Remelli[b,*]

[a] *Dipartimento di Scienze Chimiche, della Vita e della Sostenibilità Ambientale, Università di Parma, Parco Area delle Scienze 11/A, 43124 Parma, Italy. E-mail: matteo.tegoni@unipr.it*

[b] *Dipartimento di Scienze Chimiche e Farmaceutiche, Università di Ferrara, via Luigi Borsari 46, 44121 Ferrara (Italy). E-mail: rmm@unife.it*

 # Current address: Institute of Inorganic Chemistry, University of Zurich, Winterthurerstrasse 190, 8057 Zurich, Switzerland

** M.T. and M.R. equally contributed to this work*

*Corresponding authors:

Matteo Tegoni, e-mail: matteo.tegoni@unipr.it; phone +39 0521 905424; fax: +39 0521 905557

Maurizio Remelli, E-mail: rmm@unife.it; phone: +39 0532 455150; fax: +39 0532 240709

Abstract

The two branched peptides $(AAHAWG)_4$-**PWT2** and $(HAWG)_4$-**PWT2** where synthesized by mounting linear peptides on a cyclam-based scaffold (**PWT2**), provided with four maleimide chains, through a thio-Michael reaction. The purpose of this study was primarily to verify if the two branched ligands had a Cu(II) coordination behaviour reproducing that of the single-chain peptides, namely AAHAWG-NH_2, which bears an Amino Terminal Cu(II)- and Ni(II)-Binding (ATCUN) Motif, and HAWG-NH_2, which presents a His residue as the N-terminal amino acid, in a wide pH range. The study of Cu(II) binding was performed by potentiometric, spectroscopic (UV-vis absorption, CD, fluorescence) and ESI-MS techniques. ATCUN-type ligands ($(AAHAWG)_4$-**PWT2** and AAHAWG-NH_2) were confirmed to bind one Cu(II) per peptide fragment at both pH 7.4 and pH 9.0, with a [NH_2, $2N^-$, N_{Im}] coordination mode. On the other hand, the ligand HAWG-NH_2 forms a $[CuL_2]^{2+}$ species at neutral pH, while, at pH 9, the formation of 1:2 Cu(II):ligand adducts is prevented by amidic nitrogen deprotonation and coordination, to give rise solely to 1:1 species. Conversely, Cu(II) binding to $(HAWG)_4$-**PWT2** resulted in the formation of 1:2 copper:peptide chain also at pH 9: hence, through the latter branched peptide we obtained, at alkaline pH, the stabilization of a specific Cu(II) coordination mode which results unachievable using the corresponding single-chain peptide. This behaviour could be explained in terms of high local peptide concentration on the basis of the speciation of the Cu(II)/single-chain peptide systems.

Keywords

Metal complexes; copper(II); branched peptides; cyclam scaffold; solution equilibria; peptide welding technology.

INTRODUCTION

Branched peptides have been explored in recent years for the isolation of compounds capable of nucleic acid condensation [1, 2] and gene delivery [3-5], characterized by a high resistance to peptidases [6, 7] or with application in multivalent interactions with biomolecular targets [8, 9]. In the last decade, branched peptides and more in general oligopeptides covalently mounted on a molecular scaffold were explored for their metal-binding properties [10].

Among those presented in the literature, branched peptides studied for metal binding are profoundly diverse in complexity. Examples were given of short dipeptides [11-14] and long oligopeptides that spontaneously fold into supersecondary structures such as coiled coils [15-17]. For this latter class of peptides the term template-assisted synthetic protein (TASP) was coined [18]. All these peptides operate metal binding in a diverse way depending on the amino acid composition and preorganization or fold of the overall branched peptide. As a general observation, the branches in a branch peptide act as independent metal binding moieties for less structured constructs, while single metal binding sites could be obtained for folded architectures [19].

A new, relatively simple and very efficient method for the synthesis of tetrabranched peptides has been recently described [20]. It guarantees very high yields and an excellent purity of the products. The synthetic strategy was named “peptide welding technology” (PWT) and it consists of fixing four identical peptides on a suitable scaffold, by means of a convergent approach. First, the peptide sequence and the scaffold are separately synthesized and purified; then, they are bonded together by exploiting the presence of specific mutually-reactive functional groups. The thiol-Michael reaction, which is highly chemoselective, was used for this PWT strategy. The peptide contains an additional C-terminal cysteine residue and the reaction occurs between the Cys thiolic side chain and a α-β-unsaturated carbonyl group present on the platform, thus a thio-ether addition product is obtained. Among several studied cores, we focused our attention on the so called **PWT2**, a scaffold based on the cyclam (1,4,8,11-tetraazacyclotetradecane) moiety, - where four maleimide chains are linked through a spacer to the four nitrogen atoms of the hetero-cycle (Scheme 1).

In this paper we present two branched homomeric tetrapeptides consisting of four linear tetra- or hexa-peptides mounted on a **PWT2** scaffold, capable of binding Cu(II) at their N-termini (Scheme 1). The used linear peptides were AAHAWGC-NH_2 and HAWGC-NH_2. The C-terminal Cys present in each peptide had the thiol function converted into a thioether group as a consequence of the covalent linkage to the cyclam scaffold (Scheme 1). Furthermore, these peptides are characterized by the presence of one histidine residue as the principal metal binding residue, and were designed to achieve the stabilization of two different metal coordination environments, as discussed below. The tetrameric ligand $(AAHAWG)_4$-**PWT2** contains four ATCUN (Amino Terminal Cu(II)- and Ni(II)-Binding Motif) N-termini, corresponding to the Xxx-Xxx-His- sequence, while the ligand $(HAWG)_4$-**PWT2** has a histidine as first amino acid at its four N-termini. These ligands are therefore homomeric branched tetrapeptides with four or six residues plus a spacer between the peptide and the scaffold. Conversely to the examples in literature [21], these ligands ensure a high degree of flexibility of the construct and the possibility to bind either four metal ions (one per arm) or two metal ions (two peptides coordinated to each metal).

The rationale for the use of these ligands is the following: peptides with ATCUN sequence are known to form 1:1 Cu(II)/peptide adducts with a (NH_2, $2N^-$, N_{Im}, Scheme 2a) metal coordination [22-24]. In addition, this binding mode is known to be stable over a quite wide pH range. On the contrary, peptides containing the amino-terminal His residue have been reported to form different complexes with Cu(II) as a function of the pH. In particular, a (2N) mode – known as *histamine-like* mode (Scheme 2b) – or a (N, O) coordination mode – which we can call *glycine-like* mode, for the sake of simplicity, (Scheme 2c) – are expected to be stable at low pH [25-27]. The deprotonation of the peptide nitrogen atoms of the backbone and subsequent coordination to Cu(II) has been observed at higher pH values [28, 29]. Here we aimed to take advantage of anchoring of four short peptides to a single scaffold to stabilize specific Cu(II) coordination environments. In particular, we aimed to evaluate if with $(HAWG)_4$-**PWT2** – considering the high local concentration of peptides – a *histamine-like* coordination of the N-terminal His could be stabilized at pH values where, using single-chain peptides, it cannot be formed.

Along with the two branched peptides, in this work we have studied the corresponding single-chain peptides, containing or not a Cys(SMe) residue at their C-terminus to simulate the role played by the spacer in the tetrameric ligands (Scheme 3). The thermodynamic speciation model in solution, in a wide pH range, was obtained through potentiometric titrations and the

stoichiometry of the formed species was confirmed by mass spectrometry. A deep spectroscopic investigation with several different techniques allowed to formulate structural hypotheses for the complexes formed in solution, under different experimental conditions.

EXPERIMENTAL

Reagents

Synthesis and purification of the ligands

Tetrabranched peptide derivatives were prepared using a convergent synthetic approach previously optimized and employed by our research group for the synthesis of a series of G-protein coupled receptor ligands [20]. Linear peptides were synthesized by solid phase method with an automatic solid phase peptide synthesizer Syro II (Biotage, Uppsala Sweden) using Fluorenylmethyloxycarbonyl (Fmoc)/tBu chemistry [30]. The resin 4-(2',4'-dimethoxyphenyl-Fmoc-aminomethyl)-phenoxyacetamido-norleucyl-4-Methylbenzhydrylamine (Rink amide MBHA resin) was used as a solid support.

As an example, for the synthesis of AAHAWGC-NH_2, the following procedure was applied. The resin was treated with 40% piperidine/*N,N*-dimethylformamide (DMF) and linked with Fmoc-Cys(Trt)-OH (Trt = Trityl = Triphenylmethyl) by using [O-(7-azabenzotriazol-1-yl)-1,1,3,3-tetramethyluronium hexafluorophosphate] (HATU) as the coupling reagent. The following Fmoc amino acids were sequentially coupled to the growing peptide chain: Fmoc-Gly-OH, Fmoc-Trp(Tert-butyloxycarbonyl = Boc)-OH, Fmoc-Ala-OH, Fmoc-His(Trt)-OH, Fmoc-Ala-OH, Fmoc-Ala-OH. All the Fmoc amino acids (4 equiv.) were coupled to the growing peptide chain by using HATU (4 equiv.) in DMF in the presence of an equimolar concentration of 4-methylmorpholine (NMM), and the coupling reaction time was 1 h. To improve the analytical profile of the crude peptide, capping with acetic anhydride (0.5 M/DMF) in the presence of NMM (0.25 M/DMF) (3:1 v/v; 2 mL / 0.2 g of resin) was performed at any step. 40% Piperidine/DMF was used to remove the Fmoc protecting group. The protected peptide-resin was treated with reagent B [31] (trifluoroacetic acid (TFA)/H_2O/phenol/triisopropylsilane 88 : 5 : 5: 2; v/v; 10 mL / 0.2 g of resin) for 1.5 h at room temperature. After filtration of the resin, the solvent was concentrated *in vacuo* and the residue triturated with ether. Crude peptide was purified by preparative reversed-phase HPLC using a Water Delta Prep 3000 system with a Jupiter column C_{18} (250 x 30 mm, 300 A, 15 µm spherical

particle size). The column was perfused at a flow rate of 20 mL/min with a mobile phase containing solvent A (5% v/v acetonitrile/water, 0.1% TFA), and a linear gradient from 0 to 60% of solvent B (60% v/v acetonitrile/water, 0.1% TFA) over 25 min for the elution of peptides.

In order to obtain the branched peptide $(AAHAWG)_4$-**PWT2**, purified AAHAWGC-NH_2 x TFA (37 mg; 0.044 mmol) was reacted in solution (H_2O/CH_3CN 1/1; 2 mL) with **PWT2** [20] core (8.6 mg; 0.01 mmol) in the presence of 100 µL of 5% $NaHCO_3$ in a classical thio-Michael reaction previously optimized for the synthesis of Nociceptin/orphanin FQ tetra branched derivatives [32]. As expected, the reaction reached completion in a few minutes and the mixture was directly purified by preparative HPLC using experimental condition previously reported for the purification of the linear peptide. The compound $(HAWG)_4$-**PWT2** was synthesized in a similar manner.

Analytical HPLC analyses were performed on a Beckman 116 liquid chromatograph equipped with a Beckman 166 diode array detector. The analytical purity of the final compounds (the branched: $(AAHAWG)_4$-**PWT2**, $(HAWG)_4$-**PWT2** and the linear: AAHAWG-NH_2, HAWG-NH_2, AAHAWGC-NH_2, HAWGC-NH_2, AAHAWGC(SMe)-NH_2, HAWGC(SMe)-NH_2,) was determined using a Luna C_{18} column (4.6 x 100 mm, 3 µm particle size) with the above solvent system (solvents A and B) programmed at a flow rate of 0.5 mL/min using a linear gradient from 0% to 70% B over 25 min. Final products showed ≥ 95% purity when monitored at 220 nm. Molecular weights of final compounds were determined by a mass spectrometer ESI Micromass ZMD-2000 (Waters®).

The tetra-acetylated cyclam-based scaffold 1,1',1'',1'''-(1,4,8,11-tetraazacyclotetradecane-1,4,8,11-tetrayl)tetraethanone (Ac_4-cyclam) was obtained by dissolving 1,4,8,11-tetraazacyclotetradecane (1.0 mmol) in acetic anhydride (2 mL). The reaction was then left to stir overnight. After this time, the solvent was removed under vacuum and the crude product was purified via silica gel column chromatography using EtOAc as eluent. ^{1}H and ^{13}C NMR measurements confirmed the synthesis of Ac_4-cyclam, giving the following values of chemical shift: 1H NMR (400 MHz, DMSO-d6) = δ 3.58-3.25 (m, 16H), 2.03-1.66 (m, 12H), 1.92-1.62 (m, 4H); 13C NMR = δ 170.03, 169.99, 169.84, 169.68, 48.37, 48.05, 47.19, 46.66, 45.71, 44.90, 44.44, 43.72, 43.10, 28.09, 27.63, 27.12, 21.34, 20.77.

Solution studies

All the linear and branched peptide solutions were prepared in freshly-boiled bidistilled water, in the presence of HCl 2 mM; the peptide (single chain) concentration was always about 10 mM. The

stock solution of Ac_4-cyclam was prepared in D_2O and its concentration (19.1 mM) was determined by H^1-NMR using an external standard (L-Phe).

Potentiometric measurements

The potentiometric titrations of AAHAWG-NH_2, HAWG-NH_2, AAHAWGC(SMe)-NH_2 and HAWGC(SMe)-NH_2 were carried out in aqueous solution at $T = 25 \pm 0.1$ °C and $I = 0.1$ M (KCl) under N_2 stream, using 2.2 mL samples. The potentiometric apparatus was previously described [33]. The Hamilton combined glass electrode (P/N 238000) was calibrated in terms of $[H^+]$ by titrating HCl solutions with a 0.1 M carbonate-free standardized solution of KOH and the pK_w value resulted to be 13.76(1). Protonation data were obtained by alkalimetric titration of 3 samples (C_L = 1.2-1.3 10^{-3} M). Formation constants for the Cu(II) complexes were determined from 3 titrations carried out on sample solutions where the total concentration of metal ranged from 0.5 to 1.1 mM and the copper/ligand molar ratio ranged from 1:2 to 2:1. All the systems were studied between pH 3 and 11.

The protonation and complex-formation constants of the systems were calculated with the software HyperQuad 2013 [34] and the results were used to draw the species distribution curves with the software Hyss 2009 [35].

UV-visible and Circular Dichroism data

UV and visible spectra of the Cu(II)/AAHAWG-NH_2, Cu(II)/HAWG-NH_2, Cu(II)/$(AAHAWG)_4$-**PWT2** and Cu(II)/$(HAWG)_4$-**PWT2** systems were collected with a spectrophotometer Evolution 260 Bio (Thermo Scientific, Waltham, MA, USA) provided with a Peltier thermostat, using quartz cuvettes of 1 cm path length. The absorption spectra of the Cu(II)/AAHAWGC(SMe)-NH_2 and Cu(II)/HAWGC(SMe)-NH_2 systems were recorded on a Varian Cary50 Probe spectrophotometer, using quartz cuvettes with an optical path of 1 cm. For the studies performed at fixed pH, aqueous HEPES 25 mM (pH 7.0 for Cu(II)/HAWG-NH_2; pH 7.4 for Cu(II)/AAHAWG-NH_2) or CHES 25 mM (pH 9.0) were employed. The used Cu(II) and peptide concentrations were $C_{peptide}$= 0.70 mM, Cu:peptide = 0–1.32 : 1. Studies at variable pH were performed by direct addition of NaOH. Spectra were collected every half pH unit between pH 3 and 11 (Cu:peptide = 1 : 1.3–1.4, C_{Cu}= 0.50 mM). Spectrophotometric titrations of the Cu(II)/$(AAHAWG)_4$-**PWT2** and Cu(II)/$(HAWG)_4$-**PWT2** systems were performed only at fixed pH, under the conditions used for linear peptides, by the addition of Cu(II) aliquots to the buffered ligand solutions (C_{ligand}= 0.17 mM, Cu:ligand = 0–8.2 : 1).

CD spectra of the Cu(II)/AAHAWG-NH_2, Cu(II)/HAWG-NH_2, Cu(II)/$(AAHAWG)_4$-**PWT2** and Cu(II)/$(HAWG)_4$-**PWT2** systems were collected with a Jasco J715 spectropolarimeter, using 0.1 and 1 cm path length cuvettes for the UV and the Vis range, respectively. CD data collection at variable pH for Cu(II)/AAHAWG-NH_2 and Cu(II)/HAWG-NH_2 was performed between pH 3.2 and 12 by direct addition of NaOH. For spectra collected in the UV region the concentrations were Cu:peptide= 1 : 2–2.2, C_{Cu}= 48–52 μM; for spectra collected in the visible region the concentrations were Cu:peptide= 1 : 2–2.2, C_{Cu} = 0.48-0.52 mM. CD data collection at fixed pH was performed at pH 7.4 for Cu(II)/AAHAWG-NH_2 and pH 7.0 or pH 9.0 for Cu(II)/HAWG-NH_2. The same buffer conditions of absorption measurements were employed. The Cu(II)/$(AAHAWG)_4$-**PWT2** and Cu(II)/$(HAWG)_4$-**PWT2** systems were studied only at fixed pH (7.4 and 9.0 for the former, 7.0 for the latter, same buffer solutions as above). For both UV and visible regions, the following conditions were employed: C_{ligand}= 0.20 mM, Cu:ligand = 0–4 : 1. For Cu(II)/$(AAHAWG)_4$-**PWT2**, opalescence was observed at pH 9.0 for Cu(II):ligand greater than 1. For Cu(II)/$(HAWG)_4$-**PWT2**, opalescence was observed at pH 9.0 upon addition of small quantities of Cu(II), which prevented the collection of reliable CD data. CD data at pH 7.0 for $(HAWG)_4$-**PWT2** were limited to Cu:ligand = 0–4 : 1 due to opalescence for higher amounts of Cu(II).

Spectrofluorometric titrations

Emission spectra were collected on a Horiba Jobin Yvon Fluoromax 3 spectrofluorimeter, using a 1 cm path length quartz cuvette. The protonation equilibria of AAHAWG-NH_2 and HAWG-NH_2 were studied in aqueous solution between pH 3 and 10.5 by addition of small aliquots of concentrated NaOH to an acidic solution of the ligands (C_L= 9.5 and 4.8 μM for the two peptides, respectively, I = 0.1 M (KCl), T = 298.2 K). The Cu(II)/AAHAWG-NH_2 and Cu(II)/HAWG-NH_2 systems were studied at fixed pH (7.4 for the former, 7.0 and 9.0 for the latter) by titration of the peptide solution with Cu(II) (C_L= 48 μM, Cu(II)/peptide= 0–1.46). The Cu(II)/$(AAHAWG)_4$-**PWT2** and Cu(II)/$(HAWG)_4$-**PWT2** systems were studied at fixed pH (7.4 for the former, 7.0 and 9.0 for the latter) by titration of the peptide solution with Cu(II) (C_L= 20 μM, Cu/ligand= 0–5). Buffer conditions were the same as described above for absorption studies. Buffer solutions used to prepare the samples were passed through a 0.45 μm nylon filter immediately prior their use.

^{1}H-NMR

^{1}H-NMR spectra were collected on a Bruker AVANCE 400 MHz spectrometer. The Ac_4-cyclam system was studied with ^{1}H-NMR and ^{1}H-COSY (C_L = 19.1 mM in D_2O). The variable temperature spectra were collected from 25 to 75 °C. The ^{1}H-NMR spectrum in the presence of an equimolar amount of Cu(II) was also collected. The 2D spectra were collected at 75 °C. Spectra were referenced to the residual HDO peak [36].

Electrospray-Ionization Mass-Spectrometry (ESI-MS)

ESI mass spectra were recorded on a linear ion trap LTQ XL Mass Spectrometer (Thermo Scientific, Waltham, MA, USA). Data were processed by using the spectrometer software. The measurements were performed on binary metal/ligand solutions at appropriate pH values, chosen in order to maximize the formation of a single complex species. The samples were prepared in a similar way as described for potentiometric studies without the addition of background electrolyte, in water/methanol 50:50 V/V. The counter-ion was supplied by the base employed to adjust the pH value (KOH). Direct infusion analyses were always performed at 5 µL/min. Experimental conditions were as follows: spray voltage 4.8 kV; sheath gas 40 a.u.; capillary temperature 250 °C; capillary voltage 8-25 V and tube lens 60-120 V.

RESULTS

Study of Cu(II) / Ac_4-cyclam system

The compound Ac_4-cyclam has been synthesized and used as a model to study the possible binding of Cu(II) to the functionalized cyclam scaffold. Ac_4-cyclam has been characterized by ^{1}H-NMR and ^{1}H-COSY experiments (Figs. S1 and S2, Supplementary Information). Multiple peaks are present in the 1.5–2.2 ppm (alkyl C-CH_2-C and acyl CH_3CO protons) and 3.3–3.8 ppm ranges (CH_2-N protons). Increasing the temperature up to 75 °C, we observed progressive broadening of the alkyl signals and coalescence of the acyl ones (Fig. S2, Supplementary Information). These data overall demonstrate that the conformation of the scaffold is fluxional in intermediate exchange on the NMR time scale with prevalence of slow exchange at 25 °C.

The acid-base behaviour of Ac_4-cyclam has been investigated by potentiometry. The obtained titration curve (Fig. S3, Supplementary Information) is nicely superimposable to that calculated for the titration of HCl alone, without Ac_4-cyclam. This result confirms that Ac_4-cyclam

does not have any acid-base activity which could interfere with the potentiometric study of the apo-peptidic chains. Furthermore, in order to exclude Cu(II) binding to Ac_4-cyclam, a series of UV-Vis spectra have been recorded at different metal/ligand ratios. No changes in the wavelength of maximum of absorption have been observed and the obtained λ_{max} = 815 nm is consistent with the presence of solely Cu(II) aqua ion (Fig. 1). Further evidence comes from the NMR spectra of Ac_4-cyclam registered in the absence and in the presence of an equimolar amount of Cu(II) (Fig. S4, Supplementary Information), since signals broadening, expected for the presence of coordinated Cu(II), are completely absent.

Ligand protonation equilibria

The protonation constants of the single-chain peptides are reported in Table 1; the corresponding distribution diagrams are reported as Supplementary Information (Figs. S5 – S8).

All the linear peptides bear two basic sites, i.e. the terminal amine and the side imidazole of the His residue. Data of Table 1 are *macro*-constants and the corresponding *micro*-constants are not available; however, on the basis of literature [37] the highest log*K* value can be mainly attributed to the former functional group and the lowest to His. The protonation equilibria of AAHAWG-NH_2 and HAWG-NH_2 have also been investigated by means of spectrofluorimetric titrations and the results are shown in Fig. S9 (Supplementary Information): interestingly, the intensity of the emission band of the indole group of Trp increases as a consequence of imidazole deprotonation. As it was already previously reported [38, 39], the close proximity of a protonated histidine to tryptophan promotes a charge-transfer between the two aromatic rings which, in turn, quenches the indole fluorescence. Although this behavior is more evident for AAHAWG-NH_2 (Fig. S9a), for both AAHAWG-NH_2 and HAWG-NH_2 the assignment of the residues involved in ligand deprotonation are in agreement with the spectrofluorimetric data.

Cu(II) complexes with AAHAWG-NH_2 and AAHAWGC(SMe)-NH_2

The complex-formation constants obtained by potentiometric studies of the single-chain peptides AAHAWG-NH_2 and AAHAWGC(SMe)-NH_2 are reported in Table 2. The corresponding distribution diagrams are shown in Fig. 2 and Fig. S10 (Supplementary Information). For both these ATCUN-type peptides, the potentiometric titrations confirmed their high affinity for Cu(II) ion. The obtained speciation models are in very good agreement with those reported for other similar systems [40-43] (see also Table S1, Supplementary Information). Moreover, the minor behavior

difference between the two peptides (Table 2) suggests that the additional Cys(SMe) residue has a negligible impact on their Cu(II) binding ability. For this reason, only the Cu(II)/AAHAWG-NH_2 equilibria are described below.

Starting from pH 4, the interaction between Cu(II) and AAHAWG-NH_2, after a plausible anchoring of the metal ion to either the imidazole or the amine nitrogen, leads to the concerted deprotonation of two amide nitrogens of the peptide backbone to form the complex [$CuLH_{-2}$] which quickly becomes the most abundant copper species in solution, the only one present in the pH range 5.5-9.0. The coordination geometry is most likely almost planar with the [N_{NH2}, N_{Im}, $2N^-$] donor-atom set, as represented in Scheme 2a. Further deprotonation step at alkaline pH gives the [$CuLH_{-3}$]$^-$ species. Our hypothesis is that the deprotonation of the second imidazolic proton occurs to form a coordinated imidazolate ion, rather than of an axially-coordinated water molecule. Although observed as a bridging group between two metal ions, the coordination of His in the imidazolate form to one Cu(II) has been previously observed [42, 44, 45]. Here we exclude the deprotonation of axially-bound water molecule since the signal of this ion is completely absent in the ESI-MS spectra. Rather, the speciation model of Table 2 is nicely confirmed by ESI-MS spectra recorded at slightly alkaline pH, where both the [$CuLH_{-2}$] and [$CuLH_{-3}$]$^-$ complexes have been observed and recognized through isotopic pattern analysis (Fig. S11, Supplementary Information). Interestingly, a signal attributable to the transient species [$CuLH_{-1}$]$^+$ was also recorded in the ESI-MS experiments, while the formation of this complex is too small to be observed in potentiometry. It is worth of note that the experimental *m/z* ratio of the ion [$CuLH_{-3}$]$^-$ supports the loss of a proton by the ligand and rules out the formation of a hydroxo-species. Furthermore, we also exclude the deprotonation and coordination of a third amidic nitrogen of the backbone on the basis of UV-visible and CD spectroscopic data (see below).

UV-visible and CD spectroscopic results are in agreement with the coordination hypotheses described above. Vis-absorption spectra (Fig. 3 and Fig. S12, Supplementary Information) show only one band centred at λ_{max}= 526 nm, compatible with the hypothesis of a 4N coordination and in particular with a [N_{NH2}, N_{Im}, $2N^-$] (expected λ_{max} = 531 nm) [46]. Such absorption band is already observable at pH 4: initially the intensity increases with pH and then remains unchanged under the most alkaline conditions. Only at pH 4 a second (weak) band is also present in the Vis spectrum, around 800 nm, due the presence of non-bound Cu(II) ions.

A spectrophotometric titration of AAHAWG-NH_2 with Cu(II) performed at pH 7.4 is shown in Fig. 4a. Increasing the Cu(II) concentration in the peptide solution from copper/ligand ratio 0 to 1,

we can observe that the absorbance at 526 nm steadily and almost linearly increases, following the formation of the complex [$CuLH_{-2}$]. In the presence of copper in excess the absorbance does not change anymore, confirming that only mono-nuclear complexes of stoichiometry 1:1 are formed in solution. Identical behaviours occurred repeating the same experiments at pH=9.0 (Fig. S13a, Supplementary Information), in full agreement with the distribution diagram shown in Fig. 2. Further confirmation of the exclusive Cu(II):peptide 1:1 binding stoichiometry has been obtained through spectrofluorimetric titrations performed in the same conditions described above: in this case, the emission intensity decreases with the formation of the complex (Fig. 4b and Fig. S13b, Supplementary Information) [46] until the Cu(II) concentration becomes equimolar to that of AAHAWG-NH_2.

The quenching of the Trp fluorescence due to the formation of copper complexes has also been evidenced by means of a further spectrofluorimetric titration of a diluted Cu(II)/AAHAWG-NH_2 solution at fixed Cu(II)/L ratio and varying the pH value from 3.5 to 11.5 (Fig. S14, Supplementary Information). The emission intensity at 350 nm decreases until pH 5.5 where the formation of the complex [$CuLH_{-2}$] is complete and then it remains stable until pH approximatively 10, when the species $[CuLH_{-3}]^-$ starts to form.

CD spectra recorded for Cu(II)/AAHAWG-NH_2 solutions in the pH range 4–12 (Fig. 5) are almost identical, confirming that the complex geometry remains unchanged when pH is varied. This observation, together with the absence of λ_{max} changes, confirm that in this pH range the coordination environment of Cu(II) is almost the same for both [$CuLH_{-2}$] and $[CuLH_{-3}]^-$. Above pH 10, deprotonation/coordination of an amide should give rise to an important change in the complex geometry and, consequently, in the CD spectra. This is not observed and, as previously discussed, we suggest the deprotonation of the pyrrole-type nitrogen of the imidazole ring of His. In the UV range of the CD spectra two main bands have been observed, one negative at 274 nm and one positive at 310 nm. The former can be attributed to an intra-ligand transition due to the indole group; the latter is the well-known charge transfer band due to the coordination of amide nitrogens to the copper ion [46, 47]. In the Vis region, the double band centred around 520 nm corresponds to the typical metal d-d transitions of a Cu(II) complex with ATCUN peptides [47, 48]. It is worth of note that the CD spectra of the Cu(II)/AAHAWG-NH_2 system are almost perfectly superimposable to that reported for the Cu(II) binding to human serum albumin (Fig. S15, Supplementary Information) [22].

Cu(II) complexes with HAWG-NH_2 and HAWGC(SMe)-NH_2

Potentiometric analyses of the Cu(II)/HAWG-NH_2 and Cu(II)/HAWGC(SMe)-NH_2 systems were performed in the presence of an excess of either the ligands (Cu/L ratio = 1 : 1.2; 1 : 2.2) or the metal (Cu/L ratio = 1.3 : 1), in the pH range 3–11. No precipitation was observed with the employed conditions. Seven mono- and di-nuclear complexes have been revealed in these systems, as reported in Table 3 and in Figs. 6 and S16 (Supplementary Information). All the species detected by potentiometry for the system Cu(II)/HAWG-NH_2 have been observed by ESI-MS, as shown in Fig. S17 and Fig. S18 (Supplementary Information). At pH=7.0 the signals corresponding to the $[CuL]^{2+}$ and $[CuL_2]^{2+}$ species can be recognized (at *m/z* = 265.58 and 499.83, respectively) along with those of the dimers $[Cu_2L_2H_{-2}]^{2+}$ (*m/z* = 531.25) and $[Cu_2L_2H_{-3}]^{+}$ (*m/z* = 1061.00). At pH=9.0 the deprotonated complexes $[CuLH_{-2}]$ and $[CuLH_{-3}]^{-}$ were observed as K^+ adducts in the positive ion mode and alone (the latter) in the negative ion mode. The obtained speciation models of Table 3 are very similar considering both the stoichiometry and the stability of the formed complexes, thus suggesting again that the Cys(SMe) residue has a minor influence on the complex-formation behavior, as already mentioned for AAHAWC(SMe)G-NH_2. Therefore, only the Cu(II)/AAHAWG-NH_2 equilibria are examined in the following paragraphs.

The peptide HAWG-NH_2 is characterized by the presence of His in the first position (amino-terminus), that can chelate the Cu(II) ion in the very effective *histamine-like* mode (Scheme 2). In fact, under the most acidic conditions, the first formed species is $[CuL]^{2+}$; its stoichiometry suggests that both the terminal amine and the side imidazole ring are unprotonated and bound to the metal ion, most likely in the equatorial plane of a distorted octahedral complex where the remaining positions are occupied by water molecules. The predicted wavelength of maximum absorption for this type of Cu(II) coordination is 675 nm [46], in very good agreement with the Vis absorption spectrum registered at pH 4.45 (λ_{max}= 676 nm), where this species is by far the most abundant in solution (Fig. 7).

In the presence of excess of peptide (Fig. 6a), at neutral or slightly alkaline pH, a second ligand binds the Cu(II) ion, leading to the formation of the $[CuL_2]^{2+}$ species, practically the only complex in solution in the pH range 6–8. Vis absorption spectra show a clear blue-shift and the wavelength of maximum absorption lowers approximately to 634 nm, suggesting the substitution of the coordinated water molecules with nitrogen donors. However, the blue-shift is too little to suggest that the second ligand also chelates copper in the *histamine-like* mode. In fact, in the case of four nitrogens bound to Cu(II) in the equatorial plane, the predicted wavelength of the

absorption band would be 559 nm [46]. On the other hand, the stoichiometry of the complex reveals that both the nitrogens of the second ligand are unprotonated. The alternative structural hypothesis for the bis-complex is that the second ligand is bound to copper in the so-called *glycine-like* mode, i.e. through its terminal amino group and the neighboring carbonyl oxygen (Scheme 2c). By admitting the presence of both coordination modes, the predicted maximum of absorption is 607-617 nm [46]. The second amino group likely binds Cu(II) in axial position, and is responsible of the small red-shift of the band, from the expected 607-617 to the observed 634 nm [46]. The "plasticity" of the Cu(II) ion makes impossible to establish which of the two nitrogens is equatorial or axial: most likely, a mixture of species with slightly different geometry is present in solution. It is worth noting that when pH is raised from 4 to 7, CD spectra in the Vis region change only in their intensity but not in their shape (Fig. 8), suggesting that the donor atom set remains the same.

Starting from pH 8.5, both Vis absorption and CD spectra undergo an abrupt change, exactly in correspondence to the formation of the species $[CuLH_{-3}]^-$ which dominates in the alkaline pH range. It is clear that an important transformation of the complex takes place and this can be attributed to a change in the donor atom set due to the availability of deprotonated amide nitrogens of the backbone. Bis-complexes are no longer present in solution, most likely because the ligand wraps completely the metal and binds it in equatorial position with three amide nitrogens and the imidazole (or the terminal amine). The predicted absorption band for these [N_{im}, $3N^-$] or [N_{NH2}, $3N^-$] coordination modes should be located at 522 or 515 respectively [46]. The experimental value (500 nm) is in reasonable agreement with this prediction. Further proof of these coordination hypotheses comes from spectrophotometric titrations of HAWG-NH_2 with Cu(II) at fixed pH = 7 and 9. The absorption values at the registered λ_{max}, *i.e.* 630 nm at pH = 7.0 and 500 nm at pH = 9.0 (Fig. 9) were monitored. At pH 7.0 the intensity of the absorption band almost linearly increases until the molar amount of copper in solution is about half of that of HAWG-NH_2**,** thus confirming the prevalence in solution of a complex with Cu/L stoichiometry 1:2. Conversely at pH 9.0 (Fig. 9b) the plateau corresponding to the maximum absorption intensity is obtained for the equimolar Cu/L solution, thus confirming the presence of a dominant species with stoichiometry 1:1 (i.e. the complex $[CuLH_{-3}]^-$, see Fig. 6).

Spectrofluorimetric titrations were performed at pH 7.0 and 9.0 showing that the emission intensity decreases when the Cu(II) concentration increases in solution, as already observed for the ligand AAHAWG-NH_2**.** Data reported in Fig. 10 are in reasonable agreement with the UV-visible

titrations and support the hypothesis of complexes with stoichiometry 1:2 at neutral pH and 1:1 under alkaline conditions.

It is worth noting that the interpretation of the spectral data is not so straightforward when the Cu/L ratio is close to 1:1. In this case, the dinuclear complexes observed in the ESI-MS spectra reach relevant concentrations (up to 40% of total copper, see Fig. 6b) and they can be detected also by potentiometry. Spectroscopic results for Cu(II)/HAWG-NH_2 and Cu(II)/HAWGC(SMe)-NH_2 with Cu/L ratio = 1 : 1.2 also confirm the possible existence of these species in the pH range 6–8 (Figs. S19 and S20, Supplementary Information), where the UV-Vis spectra slightly change compared to the Cu/L = 1:2 solution. A hydroxo-bridged nature of these dinuclear complexes can be foreseen, consistently with literature data for similar systems [48, 49].

Cu(II) complexes with $(AAHAWG)_4$-PWT2

With the speciation of the single-chain peptides in our hands, we studied the interaction of Cu(II) with the two tetramers built on the cyclam scaffold through spectroscopic and spectrometric techniques at fixed pH.

The mass spectrum at pH 4.9 of the ligand $(AAHAWG)_4$-**PWT2** (Fig. S21a, Supplementary Information), exhibits an excellent protonation pattern: all the species from LH_2^{2+} to LH_8^{8+} have been detected, accompanied by one or more additional signals at + 60/z, attributable to adducts [Na^+ + K^+ - 2H^+] (23 + 39 - 2 = 60), with the same charge of the purely protonated ions. In the presence of a four-fold excess of Cu(II), both at pH 7.2 and 9.8, the only two recognizable complexes are the species $[Cu_4LH_{-8}]K_4^{4+}$ (m/z = 1029.4) and $[Cu_4LH_{-8}]K_3^{3+}$ (m/z = 1359.7), suggesting that each branch of the tetramer behaves exactly like the monomer and independently binds one Cu(II) ion (Fig. S21b, Supplementary Information). This hypothesis is confirmed by spectrophotometric and spectrofluorimetric titrations performed at pH 7.4 (Fig. 11). Actually, at pH 7.4 the absorbance increases and the fluorescence intensity decreases during the addition of Cu(II), reaching a plateau when the metal ion is equimolar to the peptide branches, i.e. when the concentration of copper is four times that of $(AAHAWG)_4$-**PWT2.** Accordingly, the CD spectra recorded at pH 7.4 in the presence of increasing amounts of Cu(II) have the same shape of those recorded for the system Cu(II)/AAHAWG-NH_2, confirming the same coordination behavior (Fig. S22, Supplementary Information). Similar spectrofluorimetric data were obtained at pH 9.0, while spectrophotometric and CD data could be collected only up to 1 eq. of Cu(II) due to appearance of opalescence in the solution (Figs. S23 and S24, Supplementary Information). The λ_{max} at 500-515

nm in the absorption spectra, together with CD information, reveals that also at this pH the ATCUN nature of the copper coordination systems at both pH values examined.

Cu(II) complexes with $(HAWG)_4$-PWT2

The mass spectrum recorded at pH 3.7 for the ligand $(HAWG)_4$-**PWT2**, in the absence of metal ions, contains all the protonated species, from LH_2^{2+} to LH_5^{5+}; the presence of Na^+ or K^+ adducts is negligible (Fig. S25, Supplementary Information). In the presence of a 2:1 excess of Cu(II), the solution was light-blue colored, both at neutral and alkaline pH. The mass spectra show the signals of both mono- and bi-nuclear species, variously protonated (Fig. S26, Supplementary Information). Deprotonated and hydroxylated species, respectively $[Cu_2LH_{-1}]^{3+}$ (m/z = 1091.1) and $[Cu_2L(OH)]^{3+}$ (m/z = 1097.1), can be observed at pH=9.1. On the other hand, when Cu(II) was present in a four-fold excess, the solution was pink and not perfectly clear at pH higher than 6.7. The signals of both three- and tetra-nuclear complexes are present in the MS spectrum (Fig. S27, Supplementary Information).

The spectrofluorimetric titration curve in Fig. 12a shows that, at pH 7, the tryptophan emission steadily decreases until the Cu(II)/$(HAWG)_4$-**PWT2** ratio reaches the value of 2 and it remains constant at higher values. This behavior suggests that Cu(II), at neutral pH, forms bis-complexes with the HAWG chains (and then two copper atoms for each **PWT2**), exactly the same behaviour described above for the free HAWG-NH_2 peptide. At pH 9 (Fig. 12b) the emission decrease continues beyond the ratio Cu(II)/$(HAWG)_4$-**PWT2** = 2 until M/L ratio ca. 4. Perhaps most importantly, the equivalence point obtained from the analysis of the binding isotherm is 2 equivalents of Cu(II) per ligand $(HAWG)_4$-**PWT2**. These data suggest that at pH 9.0 the ligand $(HAWG)_4$-**PWT2** preferentially binds 2 equivalents of copper(II), in conditions where 4 Cu(II) ions are instead expected to bind, one per HAWG arm. On the other hand, the binding of four Cu(II) is promoted by the presence of an excess of Cu(II), as suggested by ESI-MS data (Fig. S27, Supplementary Information) and by fluorescence data which reach a plateau only for 4 eq. of copper added.

To further support the hypothesis of formation of Cu(II)/ligand 2:1 species both at pH 7.0 and at pH 9.0 we carried out absorption and CD studies. Complete spectrophotometric titrations of the ligand with Cu(II) was possible only at pH 7.0, since at pH 9.0 a marked drift in the baseline followed by turbidity appeared already at Cu(II):ligand of 0.3. The spectra are reported in Fig. 13. Only at pH 7.0 the visible CD spectra for addition of Cu(II) up to 4 eq. vs. ligand could be collected

(Fig. S28, Supplementary Information). At pH 7.0 the maximum of absorbance upon addition of Cu(II) is 630 nm, the same found for the system Cu(II)/HAWG-NH_2 at the same pH. Also, the corresponding CD spectrum exhibits a positive Cotton effect at 685 nm, again in agreement with the behavior of the single-chain HAWG-NH_2 peptide (Fig. S28, Supplementary Information). These results confirm that the complexation mode of $(HAWG)_4$-**PWT2** towards the Cu(II) ion, at neutral pH, is similar to that of the HAWG-NH_2 monomer, as already suggested by emission spectra described above.

Most importantly, also the spectra at pH 9.0 also present a maximum of absorption around 630 nm. That maximum corresponds to the observed at pH 7.0 for both $(HAWG)_4$-**PWT2** and HAWG-NH_2, but not of the latter at pH 9.0 (500 nm). Overall these spectroscopic data suggest that, at least in the presence of up to 2 eq. of copper, $(HAWG)_4$-**PWT2** may form 1:2 Cu : peptide complexes. This observation is fully consistent with spectrometric data (Fig S25 and S26, Supplementary Information). Also, these results suggest that, in that species the coordination environment of copper is similar to that observed for $(HAWG)_4$-**PWT2** and HAWG-NH_2 at pH 7.0 (*histamine-like* and *glycine-like* coordinated peptide arms).

DISCUSSION

In this study we present the complex-formation behavior of the two short peptides AAHAWG-NH_2 and HAWG-NH_2 along with that of their homo-tetramers $(AAHAWG)_4$-**PWT2** and $(HAWG)_4$-**PWT2**, mounted on a cyclam scaffold. Absorption and CD spectrophotometric and mass spectrometric characterization of the Cu(II) complexes with all ligands has been performed, together with the potentiometric study of the single-chain peptides speciation.

In the case of AAHAWG-NH_2, all the experimental data agree with the hypothesis of an ATCUN-type coordination for the complex $[CuLH_{-2}]$, the most abundant species in a large pH range around neutrality. Here, the chelation to the metal is carried out by the terminal amino nitrogen, the side imidazole and two deprotonated amide nitrogen atoms (Fig. 14).

The coordination behaviour of the peptide HAWG-NH_2 is more complex, since two main coordination geometries are adopted, according to the pH conditions. At pH 7.0 and in the presence of an excess of ligand, the main species in solution is the complex $[CuL_2]^{2+}$, while in the alkaline pH range the species $[CuLH_{-3}]^-$ is predominant. It is interesting to note that these two

species do not differ only in their stoichiometry but also in their coordination geometry. In fact, in the case of $[CuL_2]^{2+}$, one ligand chelates Cu(II) in the *histamine-like* mode while the other is bound to copper in the *glycine-like* mode, as suggested by visible absorption spectra. The coordination environment of Cu(II) mainly involves (3N, O) in the equatorial plane, with a possible interaction in the axial position with the imidazole nitrogen, as suggested by spectroscopic data (Fig. 15). Conversely, in the alkaline pH range the deprotonation of three amide nitrogen atoms of the peptide backbone occurs and the ligand wraps around the metal, with the participation of the terminal amine, in a (4N) coordination mode (Fig. 16). Bimetallic species, with different protonation degrees, were also detected in this system by potentiometric data analysis. These are however minor species if compared to monometallic ones, and their characterization was not carried out in further detail.

The data collected for the $(AAHAWG)_4$-**PWT2** system showed that the coordination behavior of each peptide branch parallels that of the AAHAWG-NH_2 peptide in solution. Thanks to spectroscopic measurements at fixed pH, it was possible to state that the metal forms a complex with 1:1 stoichiometry with each one of the four peptide arms anchored to the scaffold. An accurate observation of spectroscopic data for this system reveals two main features. The binding isotherm from fluorescence titration (Fig. 11) presents different slopes, with a change at 2 - 3 eq, and indicates that binding of Cu(II) ends at 3.5 equivalents of metal added to $(AAHAWG)_4$-**PWT2**. These aspects reveal that the binding of the first two metal ions is most likely non-cooperative (independent binding sites). However, after the first two-three Cu(II) eq. have been added, the coordination of further metal equivalents becomes *de facto* unfavoured either as an effect of high cations concentration or because some unidentified negative cooperative effects arise.

The behavior of $(HAWG)_4$-**PWT2** in solution was rather difficult to characterize due to insolubility problems, and nevertheless the spectroscopic data strongly suggest that 2:1 Cu / L species are formed at both pH 7.0 and 9.0, although the formation of solely 4:1 species were expected at the highest pH values. Based on fluorescence measurements at pH 7.0, we suggest the formation of a species where each metal ion is bound to two peptide arms, according to the species $[CuL_2]^{2+}$ observed for the single peptide. This means that $(HAWG)_4$-**PWT2** is saturated with two equivalents of Cu(II) *per* molecule. This hypothesis is confirmed by the Vis absorption spectra, since we observed a d-d band at 630 nm, which is very close to the λ_{max} of $[CuL_2]^{2+}$ complex of HAWG-NH_2. Moreover, CD spectra are perfectly superimposable to those recorded for the system

Cu(II)/HAWG-NH_2, at neutral pH and in excess of ligand. At neutral pH, therefore, the four HAWG chains mounted on the cyclam scaffold behave exactly like the single-chain peptides.

The same behavior has been found at pH 9.0, which deviates from what could be hypothesized from the study of Cu(II) / HAWG-NH_2 system. As predicted from our design, through $(HAWG)_4$-**PWT2** we could stabilize the formation of Cu : peptide 1:2 species, in the presence of less than 2 eq. of Cu(II). The fluorescence binding isotherm at pH 9.0 (Fig. 12b) shows that the emission intensity of the tryptophan residue is quenched very rapidly with Cu(II) addition, with an equivalence point corresponding to 2 copper ions per ligand. In these conditions the hypothesis of the formation of a 2:1 Cu:L complex (each Cu(II) coordinated by two peptide arms) is in full agreement with visible absorption data that, although affected by a marked drift of the baseline, clearly reveal that the absorption maximum of the Cu(II) adduct at this pH is above 600 nm. On the other hand, this information completely rules out the occurrence of the [N_{NH2}, $3N^-$] copper coordination found for the single-chain HAWG-NH_2 at alkaline pH. Rather, the absorption maximum is consistent with a [$2N_{NH2}$, $N_{Imidazole}$, O] coordination that we associated to the [CuL_2] species of the single-chain HAWG-NH_2 at neutral pH, as discussed.

The four arms of $(HAWG)_4$-**PWT2** are certainly different systems with respect to the free linear HAWG-NH_2 peptide. However, the spacer between the cyclam scaffold and the peptide moiety looks long enough (see below for discussion) to offer a quite high degree of freedom to the terminal peptide chain. Within the limit of the approximation of considering almost independent the four arms, as suggested by our structural models, we attempted to find an explanation for the different behavior of $(HAWG)_4$-**PWT2**, with respect to the HAWG-NH_2 simple peptide, in the stoichiometry of the species formed at high pH. Therefore, the dependence of the solution composition for the system Cu(II)/HAWG-NH_2 on the overall metal and peptide concentrations, at fixed metal/ligand ratio (1:2), has been examined. It is possible for this system due to the availability of the complete speciation model of Table 3. The main result, for Cu(II) concentrations ranging from 0.1 mM to 0.1 M, is summarized in the distribution diagram reported in Fig. S29 (Supporting Information). The diagram refers to fixed pH 9.0, for a simultaneous increasing of both the Cu(II) and peptide concentrations, at fixed Cu(II)/L = 1:2. The diagram shows that the formation of 1:2 adducts ($[CuL_2]^{2+}$ species) is predominant when the total Cu(II) concentration is above 10 mM ($\log C_{Cu(II)} > -2.0$), while for lower concentrations the $[CuLH_{-3}]^-$ species predominates. As stated above, we can cautiously transfer this information to the Cu(II)/$(HAWG)_4$-**PWT2.** Since in our experiments the $(HAWG)_4$-**PWT2** concentration is 0.20 mM (corresponding to a formal

concentration of the peptide branches of 0.80 mM), our data suggest that through $(HAWG)_4$-**PWT2** we could achieve an increase of the peptide "local concentration" [50] of 2-3 orders of magnitude compared to the same conditions using the single-chain analog. No direct experimental support is presently available for this hypothesis, due to the solubility problems of the branched peptides. An extension of the present research to more soluble peptides could give the required experimental demonstration.

Finally, we have taken into account, in evaluating our data, the presence in solution of different conformers or atropoisomers of $(HAWG)_4$-**PWT2** that surely exist as a consequence of the synthesis process (four branches are mounted on the scaffold). In this respect, conformational studies on the metal-free cyclam scaffolds reported in the literature [51], together with X ray structural data [52], suggest that N-functionalized cyclam molecules have a quite high degree of fluxionality. Under these circumstances N-linked functional groups may point away from the center of the cycle as schematically represented in Scheme 1. We analyzed the molecule with the software HyperChem 8.0 taking into account that $(CH_2)_2N\text{-}C_{acyl}$ groups are coplanar with the C=O group since it is an amidic function. A large number of conformers have been generated *in silico*, and two different atropoisomers are represented in Fig. S30 (Supporting Information). The result of the isomers analysis showed that the four branches (peptide plus spacer) have an adequate length and a sufficient degree of flexibility to place the N-termini of the peptides close to each other, allowing the formation of *histamine-like* $[Cu(peptide)_2]$ adducts.

CONCLUSIONS

In this paper we reported the synthesis of four single-chain short peptides, and two branched peptides which are template-mounted on a cyclam scaffold. All the peptides bear one histidine residue, and therefore an imidazole donor group, and a Trp residue as a spectroscopic tag. Single-chain peptides can be grouped into two couples possessing an Xxx-Xxx-His- N-terminus or a His- N-terminus, respectively. For each couple of peptides, the difference stands in the presence at the C-terminus of a Cys(S-Me) residue. This moiety simulates the thioether function present in the branched peptides as a consequence of the thio-Michael reaction used to mount the peptides on the cyclam scaffold.

Our results demonstrated that Cu(II) is bound to both the single-chain and the branched peptides preferentially at the N-termini, as previewed by our design. The ATCUN terminus in AAHAWG-NH_2 gave rise to mononuclear complexes of high stability with a $[N_{NH2}, 2N^-, N_{Im}]$

coordination. On the other hand HAWG-NH_2 formed 1:2 copper:peptide adducts at pH 7 (mixed *histamine-like* and *glycine-like* coordination), and 1:1 adducts at pH 9 where deprotonation of amidic nitrogen atoms occurred. Therefore, the major difference between the two peptides is that the ATCUN coordination mode for AAHAWG-NH_2 is stable in a wide pH range (4–10), while for HAWG-NH_2 there is a profound change of Cu(II) coordination from pH 7 to pH 9.

When mounted on the cyclam scaffold, the AAHAWG peptide retained the property to form ATCUN-type adducts with copper, as demonstrated by spectroscopic features. However, the affinity of the four chelating groups is not exactly the same, as qualitatively evidence by the spectroscopic analysis, with a decrease in chelation capacity for an increasing amount of Cu(II) bound to the ligand.

With the ligand HAWG-NH_2 we were able to qualitatively obtain what we expected from our design. On one hand, the nature of the scaffold and the length of the spacer allowed a large degree of freedom of the peptides which, at pH 7, can form 1:2 adducts with copper, adopting the mixed *histamine-like* and *glycine-like* coordination, as the single-chain peptide does. Most importantly, the latter coordination mode is predominant also at pH 9, unlike what occurs with free HAWG-NH_2. This behavior (i.e. avoiding peptide nitrogen deprotonation) is unachievable at pH 9 for the single chain-peptides unless its concentration is in the molar range. This is not only an extraordinarily high concentration for model peptides, but it is also out of the solubility range for the vast majority of proteins. Therefore, with our branched peptides we were able to shift up the effective molar concentration of the chelating groups (N-termini) of 2 to 3 orders of magnitude by mounting 4 equivalent peptides on a cyclam scaffold.

We expect that avoiding peptide nitrogen deprotonation and coordination will have, for instance, a noticeable effect on the Cu(I)/Cu(II) redox potential, since amide nitrogen coordination stabilizes Cu(II). Along with this consideration we preview that the development of these branched peptides will get into the development of copper bioinspired catalysts based on stable coordination environments at pH conditions unachievable with the use of single-chain peptides.

ACKNOWLEDGEMENTS

This work has benefited from the equipment and framework of the COMP-HUB Initiative (University of Parma), funded by the 'Departments of Excellence' program of the Italian Ministry for Education, University and Research (MIUR, 2018-2022). The financial support of University of

Ferrara (FAR 2018) and CIRCMSB (Consorzio Interuniversitario di Ricerca in Chimica dei Metalli nei Sistemi Biologici, Bari, Italy) is gratefully acknowledged.

REFERENCES

[1] H. Jiang, X.-Y. Hu, S. Mosel, S.K. Knauer, C. Hirschhäuser, C. Schmuck, ChemBioChem, 20 (2019) 1410-1416.
[2] T.J. Thomas, T. Thomas, Int. J. Biol. Macromol., 109 (2018) 36-48.
[3] M. Zhao, R. Weissleder, Med. Res. Rev., 24 (2004) 1-12.
[4] R. Sawant, V. Torchilin, Mol. Biosyst., 6 (2010) 628-640.
[5] R. Khandia, A. Munjal, A. Kumar, G. Singh, K. Karthik, K. Dhama, Int. J. Pharm., 13 (2017) 677-689.
[6] M.A. Scorciapino, I. Serra, G. Manzo, A.C. Rinaldi, Int. J. Mol. Sci., 18 (2017) 542.
[7] J.-L. Reymond, T. Darbre, CHIMIA, 67 (2013) 864-867.
[8] R. Hennig, A. Veser, S. Kirchhof, A. Goepferich, Mol. Pharm., 12 (2015) 3292-3302.
[9] A.R. Borges, C.L. Schengrund, Curr. Drug Targets: Infect. Disord., 5 (2005) 247-254.
[10] T. Yi-Hsuan, H. Adela Ya-Ting, C. Po-Yu, C. Hui-Ting, K. Chai-Lin, Curr. Pharm. Des., 17 (2011) 2308-2330.
[11] Ł. Szyrwiel, Ł. Szczukowski, J.S. Pap, B. Setner, Z. Szewczuk, W. Malinka, Inorg. Chem., 53 (2014) 7951-7959.
[12] Ł. Szyrwiel, J.S. Pap, Ł. Szczukowski, Z. Kerner, J. Brasuń, B. Setner, Z. Szewczuk, W. Malinka, RSC Advances, 5 (2015) 56922-56931.
[13] J.S. Pap, Ł. Szyrwiel, D. Srankó, Z. Kerner, B. Setner, Z. Szewczuk, W. Malinka, Chem. Commun., 51 (2015) 6322-6324.
[14] E. Farkas, D. Srankó, Z. Kerner, B. Setner, Z. Szewczuk, W. Malinka, R. Horvath, Ł. Szyrwiel, J.S. Pap, Chem. Sci., 7 (2016) 5249-5259.
[15] K. Jensen, De Novo Design of Proteins, in: K. Jensen (Ed.) Peptide and Protein Design for Biopharmaceutical Applications, John Wiley and Sons Ltd, Chirchester, UK, 2009, pp. 207-248.
[16] A.G. Tebo, V.L. Pecoraro, Curr. Opin. Chem. Biol., 25 (2015) 65-70.
[17] M. Tegoni, Eur. J. Inorg. Chem., 2014 (2014) 2177-2193.
[18] Y.C. Chen, J.D. Eisner, M.M. Kattar, S.L. Rassoulian-Barrett, K. LaFe, S.L. Yarfitz, A.P. Limaye, B.T. Cookson, J. Clin. Microbiol., 38 (2000) 2302-2310.
[19] M. Mutter, G. Tuchscherer, Cell. Mol. Life Sci., 53 (1997) 851-863.
[20] G. Calo, A. Rizzi, C. Ruzza, F. Ferrari, S. Pacifico, E.C. Gavioli, S. Salvadori, R. Guerrini, Peptides, 99 (2018) 195-204.
[21] Á. Dancs, N.V. May, K. Selmeczi, Z. Darula, A. Szorcsik, F. Matyuska, T. Páli, T. Gajda, New J. Chem., 41 (2017) 808-823.
[22] C. Harford, B. Sarkar, Acc. Chem. Res., 30 (1997) 123-130.
[23] L.W. Donaldson, N.R. Skrynnikov, W.-Y. Choy, D.R. Muhandiram, B. Sarkar, J.D. Forman-Kay, L.E. Kay, J. Am. Chem. Soc., 123 (2001) 9843-9847.
[24] J.P. Laussac, B. Sarkar, J. Biol. Chem., 255 (1980) 7563-7568.
[25] R.-P. Martin, L. Mosoni, B. Sarkar, J. Biol. Chem., 246 (1971) 5944-5951.
[26] T. Szabó-Plánka, A. Rockenbauer, L. Korecz, D. Nagy, Polyhedron, 19 (2000) 1123-1131.
[27] Y. Altun, F. Köseoğlu, J. Solution Chem., 34 (2005) 213-231.
[28] P.M.H. Kroneck, V. Vortisch, P. Hemmerich, Eur. J. Biochem., 109 (1980) 603-612.
[29] E.W. Wilson, M.H. Kasperian, R.B. Martin, J. Am. Chem. Soc., 92 (1970) 5365-5372.
[30] N.L. Benoiton, Chemistry of Peptide Synthesis, Taylor & Francis, 2005.
[31] N.A. Sole, G. Barany, J. Org. Chem., 57 (1992) 5399-5403.
[32] R. Guerrini, E. Marzola, C. Trapella, M. Pela, S. Molinari, M.C. Cerlesi, D. Malfacini, A. Rizzi, S. Salvadori, G. Calo, Biorg. Med. Chem., 22 (2014) 3703-3712.
[33] M. Quaretti, M. Porchia, F. Tisato, A. Trapananti, G. Aquilanti, M. Damjanović, L. Marchiò, M. Giorgetti, M. Tegoni, J. Inorg. Biochem., 188 (2018) 50-61.
[34] P. Gans, A. Sabatini, A. Vacca, Talanta, 43 (1996) 1739-1753.

[35] L. Alderighi, P. Gans, A. Ienco, D. Peters, A. Sabatini, A. Vacca, Coord. Chem. Rev., 184 (1999) 311-318.
[36] H.E. Gottlieb, V. Kotlyar, A. Nudelman, J. Org. Chem., 62 (1997) 7512-7515.
[37] L.D. Pettit, H.K.J. Powell, The IUPAC Stability Constants Database, Royal Society of Chemistry, London, 1992-2000.
[38] I.D.A. Swan, J. Mol. Biol., 65 (1972) 59-62.
[39] M. Shinttzky, R. Goldman, Eur. J. Biochem., 3 (1967) 139-144.
[40] D. Witkowska, S. Bielinska, W. Kamysz, H. Kozlowski, J. Inorg. Biochem., 105 (2011) 208-214.
[41] W. Bal, M. Jeżowska-Bojczuk, K.S. Kasprzak, Chemical Research in Toxicology, 10 (1997) 906-914.
[42] P. Mlynarz, D. Valensin, K. Kociolek, J. Zabrocki, J. Olejnik, H. Kozlowski, New J. Chem., 26 (2002) 264-268.
[43] C. Conato, H. Kozłowski, P. Młynarz, F. Pulidori, M. Remelli, Polyhedron, 21 (2002) 1469-1474.
[44] K. Ősz, K. Várnagy, H. Süli-Vargha, A. Csámpay, D. Sanna, G. Micera, I. Sóvágó, J. Inorg. Biochem., 98 (2004) 24-32.
[45] R.B. Martin, J.T. Edsall, J. Am. Chem. Soc., 82 (1960) 1107-1111.
[46] H. Sigel, R.B. Martin, Chem. Rev., 82 (1982) 385-426.
[47] J.M. Tsangaris, R.B. Martin, Journal of the American Chemical Society, 92 (1970) 4255-4260.
[48] H. Kozłowski, W. Bal, M. Dyba, T. Kowalik-Jankowska, Coord. Chem. Rev., 184 (1999) 319-346.
[49] R.P. Agarwal, D.D. Perrin, J. Chem. Soc., Dalton Trans., (1975) 268-272.
[50] S. Oehler, B. Müller-Hill, J. Mol. Biol., 395 (2010) 242-253.
[51] M. Meyer, V. Dahaoui-Gindrey, C. Lecomte, R. Guilard, Coord. Chem. Rev., 178-180 (1998) 1313-1405.
[52] C.R. Groom, I.J. Bruno, M.P. Lightfoot, S.C. Ward, Acta Crystallogr. B, 72 (2016) 171-179.

CAPTIONS

Scheme 1. Representation of a) the **PWT2** scaffold [20]; b) the spacer between the cyclam macrocycle and the peptide moieties; c) the tetra-acetylated cyclam-based scaffold 1,1',1'',1'''-(1,4,8,11-tetraazacyclotetradecane-1,4,8,11-tetrayl)tetraethanone (Ac_4-cyclam).

Scheme 2. Representation of a) ATCUN-type coordination; b) *histamine-like* coordination, c) *glycine-like* coordination of the peptide N-terminus to Cu(II) (R = CH_2Im).

Scheme 3. Representation of the single-chain peptides studied in this work.

Table 1. Protonation constants for the single-chain peptides at T = 298.2 K and I = 0.1 M (KCl). Standard deviations on the last figure in parentheses.

Table 2. Cumulative complex-formation constants (β) and acid dissociation constants (K_a) of Cu(II) complexes with AAHAWG-NH_2 and AAHAWGC(SMe)-NH_2, at T = 298.2 K and I = 0.1 M (KCl). Standard deviations on the last figure in parentheses.

Table 3. Cumulative complex-formation constants (β) and acid dissociation constants (K_a) of Cu(II) complexes with HAWG-NH_2 and HAWGC(SMe)-NH_2, at T = 298.2 K and I = 0.1 M (KCl). Standard deviations on the last figure in parentheses.

Fig. 1. UV-visible spectra for the titration of a water solution containing Ac_4-cyclam (19.1 mM) and $CuCl_2$ (Cu:Ac_4-cyclam ratio = 0–2).

Fig. 2. Representative species distribution diagram for complex-formation of AAHAWG-NH_2 with Cu(II), at T = 25 °C and I = 0.1 M (KCl). C_{Cu} = 1 mM; Cu:L = 1 : 1.

Fig. 3. Vis absorption spectra at variable pH of a Cu(II) / AAHAWG-NH_2 solution, at T = 25 °C and I = 0.1 M (KCl). C_{Cu} = 0.5 mM; Cu : L = 1 : 1.2. Red spectrum: pH 4.0; green: pH 4.3; blue: pH 4.6; black: pH 4.7-12.

Fig. 4. Spectrophotometric (a) and spectrofluorimetric (b) titrations of AAHAWG-NH_2 with Cu(II) at pH 7.4 (aqueous HEPES buffer 25 mM). Green dots represent: a) absorbance values at 526 nm (C_L= 0.70 mM); b) fluorescence emission data at 350 nm (λ_{exc}= 280 nm; C_L= 48 μM). Scale is reported on the right axes. Lines represent the speciation diagrams for the titration experiments (scale on the left axes). * = H_2L^{2+}; ** = L.

Fig. 5. a) UV and b) visible circular dichroism spectra at variable pH of a Cu(II) / AAHAWG-NH_2 solution, at T = 25 °C and I = 0.1 M (KCl). UV spectra C_{Cu} = 52 μM; Vis spectra: C_{Cu} = 0.52 mM; Cu:L = 1 : 2.

Fig. 6. Representative distribution diagrams for complex-formation of HAWG-NH_2 with Cu(II), at T = 25 °C and I = 0.1 M (KCl). C_{Cu} = 1 mM; a) Cu : L = 1 : 2; b) Cu : L = 1 : 1.

Fig. 7. Vis absorption spectra at variable pH for the binary solutions of HAWG-NH_2 with Cu(II), at *T* = 25 °C and *I* = 0.1 M (KCl). C_{Cu} = 0.556 mM; Cu / L = 1 : 2.2. Purple: pH 3.0; red: pH 4.5; orange: pH 7.1; cyan: pH 10.5.

Fig. 8. a) UV and b) visible circular dichroism spectra at variable pH of a Cu(II) / HAWG-NH_2 solution, at *T* = 25 °C and *I* = 0.1 M (KCl). UV spectra: C_{Cu} = 50 µM; Vis spectra: C_{Cu} = 0.52 mM; Cu/L molar ratio = 1 : 2.

Fig. 9. Spectrophotometric titrations of HAWG-NH_2 with Cu(II) at pH 7.0 (a) and at pH 9.0 (b). C_L= 0.70 mM, aqueous HEPES or CHES buffer 25 mM for pH 7.0 and 9.0, respectively. Green dots represent absorbance values. Scale is reported on the right axes. Lines represent the speciation diagrams for the titration experiments (scale on the left axes).

Fig. 10. Spectrofluorimetric titrations of HAWG-NH_2 with Cu(II) at pH 7.0 (a) and at pH 9.0 (b). C_L= 48 µM, aqueous HEPES or CHES buffer 25 mM for pH 7.0 and 9.0, respectively). Green dots represent emission values at 350 nm (λ_{exc}= 280 nm). Scale is reported on the right axes. Lines represent the speciation diagrams for the titration experiments (scale on the left axes).

Fig. 11. a) Spectrophotometric (absorbance at 522 nm, C_L= 0.17 mM) and b) spectrofluorimetric (λ_{exc}= 280 nm; λ_{emis}= 350 nm, C_L= 48 µM) titrations for a solution of $(AAHAWG)_4$-**PWT2** with Cu(II) at pH 7.4 (aqueous HEPES buffer 25 mM).

Fig. 12. Spectrofluorimetric titrations for a solution of $(HAWG)_4$-**PWT2** with Cu(II) at a) pH = 7.0 (HEPES buffer 25 mM) and b) pH = 9.0 (CHES buffer 25 mM). λ_{exc}= 280 nm; λ_{emis}= 350 nm, C_L= 48 µM.

Fig. 13. Visible spectrophotometric titrations for a solution of $(HAWG)_4$-**PWT2** with Cu(II) at a) pH = 7.0 (HEPES buffer 25 mM) and b) pH = 9.0 (CHES buffer 25 mM). C_L= 0.20 mM. The spectra at highest Cu(II) content corresponds to 4 (pH 7.0) and 0.6 eq. (pH 9.0) of Cu(II) vs. ligand, respectively.

Fig. 14. Structural hypothesis for the complex [Cu(II)(AAHAWG-NH_2)H_{-2}]. Color code: orange=copper, blue=nitrogen, red=oxygen, light grey=hydrogen, grey=carbon.**Fig. 15.** Structural hypothesis for the complex $[Cu(II)(HAWG\text{-}NH_2)_2]^{2+}$. Color code: orange=copper, blue=nitrogen, red=oxygen, light grey=hydrogen, grey=carbon.F**ig. 16.** Structural hypothesis for the complex $[Cu(II)(HAWG\text{-}NH_2)H_{-3}]^-$. Color code: orange=copper, blue=nitrogen, red=oxygen, light grey=hydrogen, grey=carbon.

Table 1

Ligand	Species	Logβ	log$K$	Residue
AAHAWG-NH_2	LH^+	7.94(1)	7.94	terminal NH_2
	LH_2^{2+}	14.30(1)	6.36	His
AAHAWGC(SMe)-NH_2	LH^+	7.86(2)	7.86	terminal NH_2
	LH_2^{2+}	14.09(3)	6.23	His
HAWG-NH_2	LH^+	7.33(5)	7.33	terminal NH_2
	LH_2^{2+}	12.89(3)	5.56	His
HAWGC(SMe)-NH_2	LH^+	7.27(3)	7.27	terminal NH_2
	LH_2^{2+}	12.58(4)	5.31	His

Table 2

Ligand	Species	Logβ	pK_a	Coordination mode
AAHAWG-NH_2	$[CuLH_{-2}]$	-0.47(1)	11.59	$[N_{NH2},N_{Im},2N^-]$
	$[CuLH_{-3}]^-$	-12.06(3)	-	$[N_{NH2},N_{Im},2N^-]$
AAHAWGC(SMe)-NH_2	$[CuLH_{-2}]$	-0.86(1)	11.7	$[N_{NH2},N_{Im},2N^-]$
	$[CuLH_{-3}]^-$	-12.6(2)	-	$[N_{NH2},N_{Im},2N^-]$

Table 3

Ligand	Species	Logβ	pK_a	Coordination mode
HAWG-NH_2	$[CuL]^{2+}$	8.24(1)	7.5	$[N_{NH2},N_{Im}]$
	$[CuLH_{-1}]^{+}$	0.7(3)	8.0	$[N_{NH2}/N_{Im},N^{-}]$
	$[CuLH_{-2}]$	-7.3(1)	7.7	$[N_{NH2}/N_{Im},2N^{-}]$
	$[CuLH_{-3}]^{-}$	-15.04(3)	-	$[N_{NH2}/N_{Im},3N^{-}]$
	$[CuL_2]^{2+}$	14.26(3)	-	$[2(N_{NH2},N_{Im})]$
	$[Cu_2L_2H_{-2}]^{2+}$	5.5(1)	7.8	
	$[Cu_2L_2H_{-3}]^{+}$	-2.3(1)	-	
HAWGC(SMe)-NH_2	$[CuL]^{2+}$	8.21(1)	7.4	$[N_{NH2},N_{Im}]$
	$[CuLH_{-1}]^{+}$	0.8(4)	7.6	$[N_{NH2}/N_{Im},N^{-}]$
	$[CuLH_{-2}]$	-6.8(1)	7.8	$[N_{NH2}/N_{Im},2N^{-}]$
	$[CuLH_{-3}]^{-}$	-14.57(4)	-	$[N_{NH2}/N_{Im},3N^{-}]$
	$[CuL_2]^{2+}$	14.63(4)	-	$[2(N_{NH2},N_{Im})]$
	$[Cu_2L_2H_{-2}]^{2+}$	5.9(1)	7.4	
	$[Cu_2L_2H_{-3}]^{+}$	-1.5(1)	-	

Scheme 1. Representation of a) the **PWT2** scaffold [20]; b) the spacer between the cyclam macrocycle and the peptide moieties; c) the tetra-acetylated cyclam-based scaffold 1,1',1'',1'''-(1,4,8,11-tetraazacyclotetradecane-1,4,8,11-tetrayl)tetraethanone (Ac_4-cyclam).

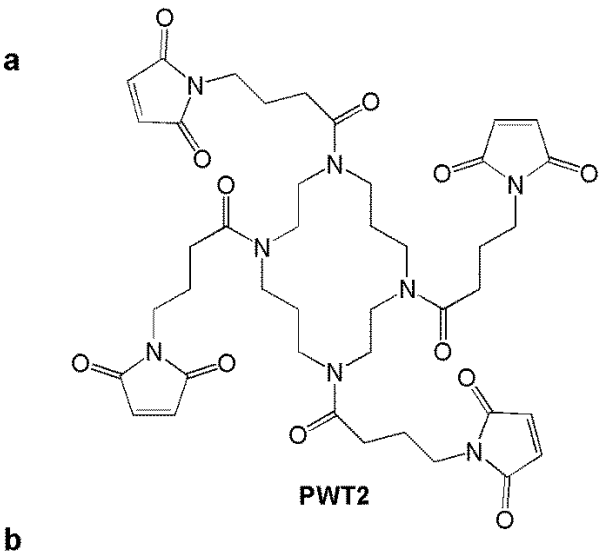

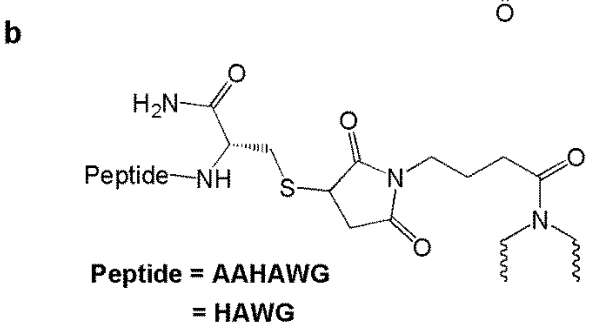

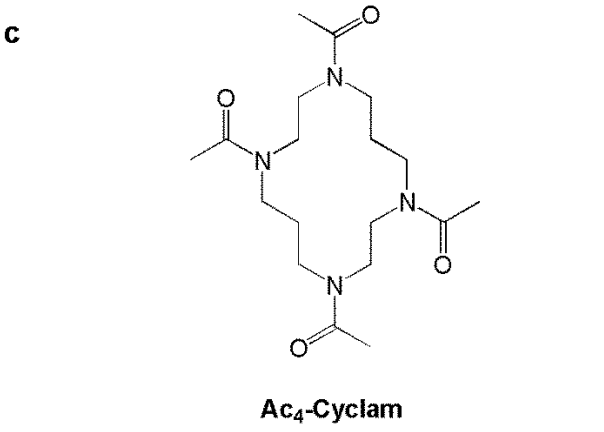

Scheme 2. Representation of a) ATCUN-type coordination; b) *histamine-like* coordination, c) *glycine-like* coordination of the peptide N-terminus to Cu(II) (R = CH_2Im).

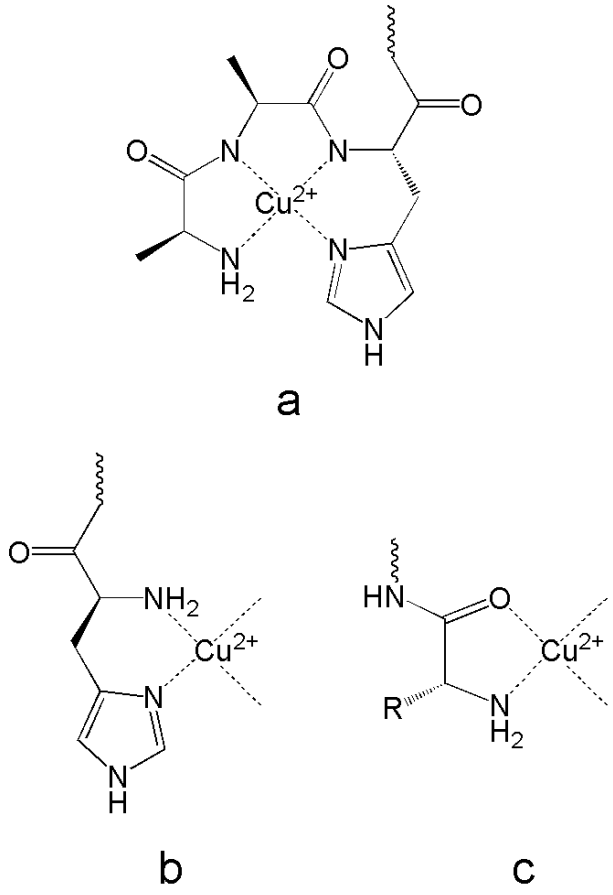

Scheme 3. Representation of the single-chain peptides studied in this work.

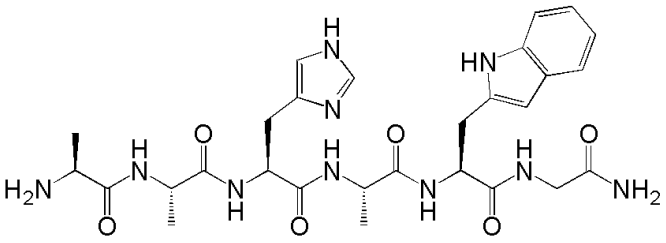

AAHAWG-NH_2

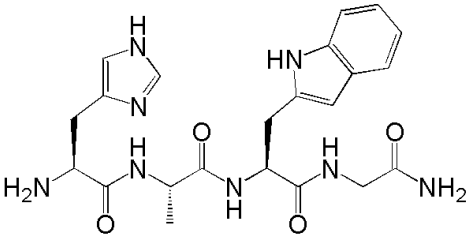

HAWG-NH_2

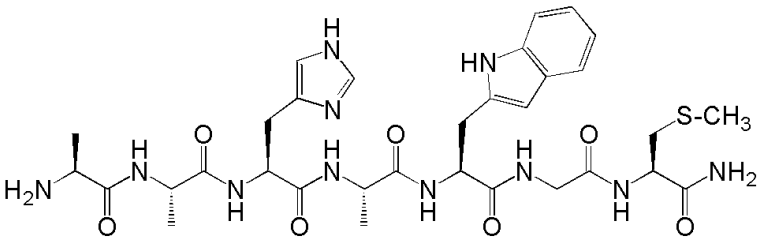

AAHAWGC(SMe)-NH_2

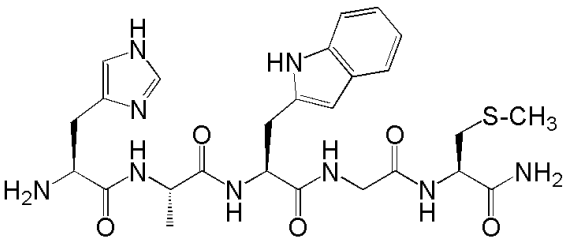

HAWGC(SMe)-NH_2

Fig. 1. UV-visible spectra for the titration of a water solution containing Ac_4-cyclam (19.1 mM) and $CuCl_2$ (Cu:Ac_4-cyclam ratio = 0–2).

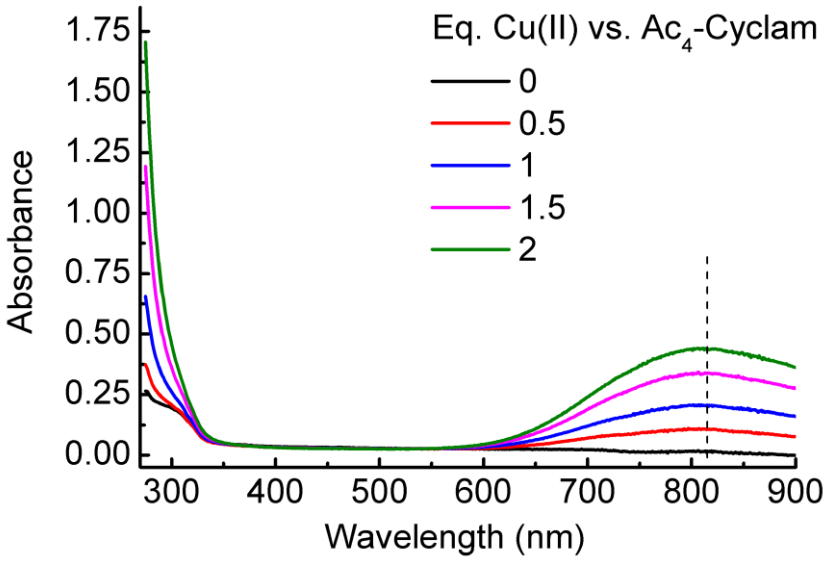

Fig. 2. Representative species distribution diagram for complex-formation of AAHAWG-NH_2 with Cu(II), at *T* = 25 °C and *I* = 0.1 M (KCl). C_{Cu} = 1 mM; Cu:L = 1 : 1.

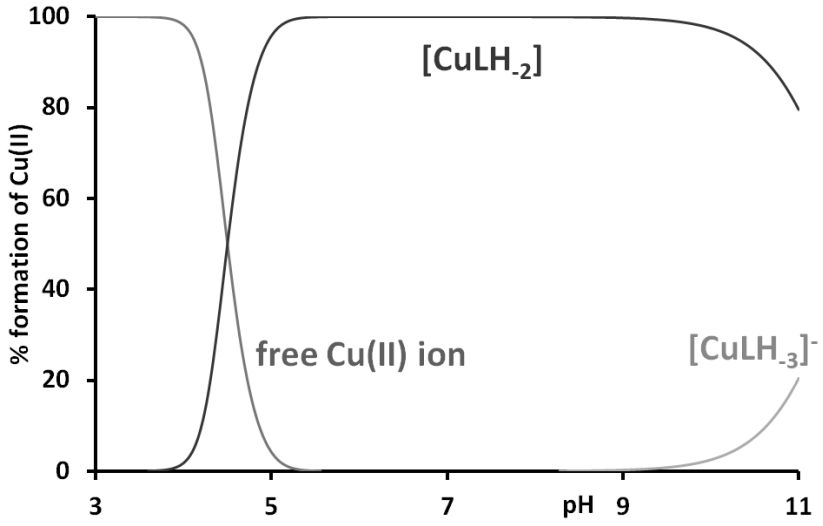

Fig. 3. Vis absorption spectra at variable pH of a Cu(II) / AAHAWG-NH_2 solution, at *T* = 25 °C and *I* = 0.1 M (KCl). C_{Cu} = 0.5 mM; Cu : L = 1 : 1.2. Red spectrum: pH 4.0; green: pH 4.3; blue: pH 4.6; black: pH 4.7-12.

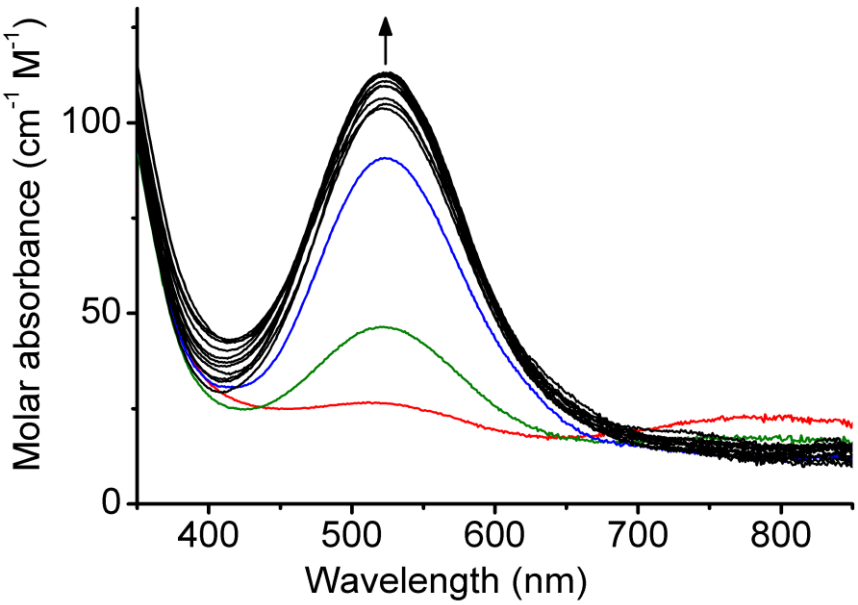

Fig. 4. Spectrophotometric (a) and spectrofluorimetric (b) titrations of AAHAWG-NH_2 with Cu(II) at pH 7.4 (aqueous HEPES buffer 25 mM). Green dots represent: a) absorbance values at 526 nm (C_L= 0.70 mM); b) fluorescence emission data at 350 nm (λ_{exc}= 280 nm; C_L= 48 µM). Scale is reported on the right axes. Lines represent the speciation diagrams for the titration experiments (scale on the left axes). * = H_2L^{2+}; ** = L.

a)

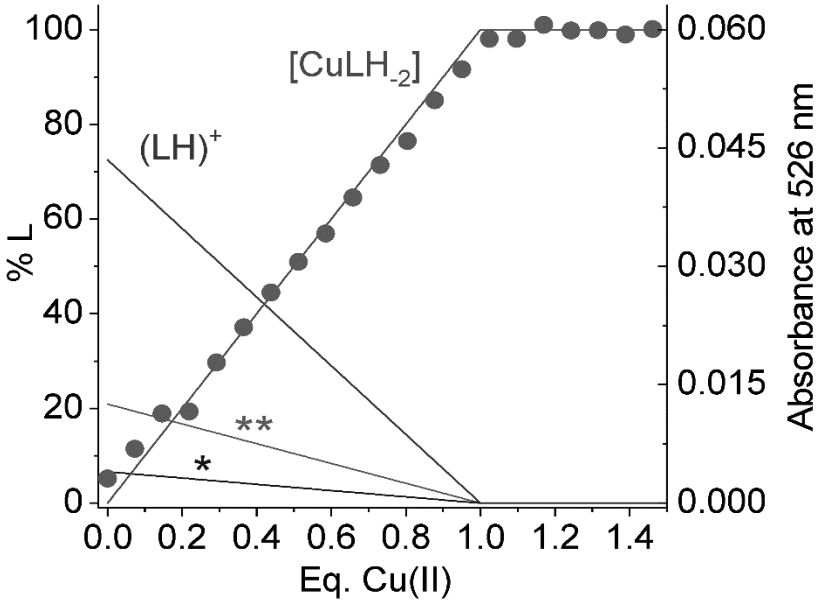

b)

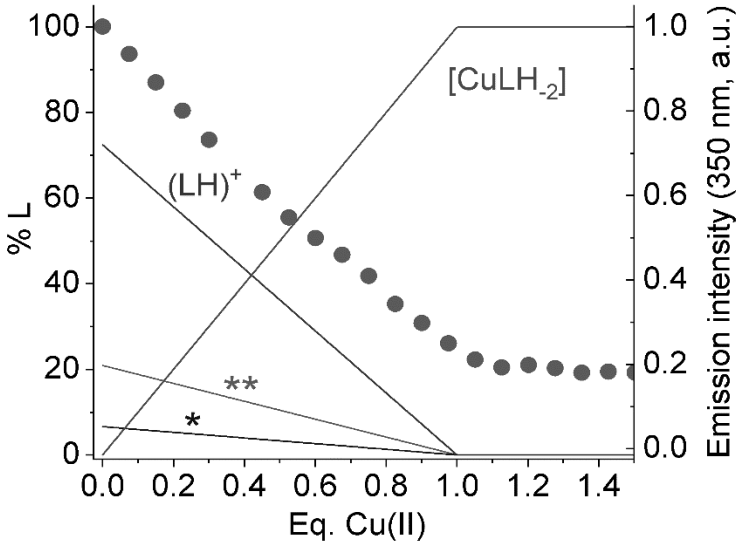

Fig. 5. a) UV and b) visible circular dichroism spectra at variable pH of a Cu(II) / AAHAWG-NH_2 solution, at *T* = 25 °C and *I* = 0.1 M (KCl). UV spectra C_{Cu} = 52 µM; Vis spectra: C_{Cu} = 0.52 mM; Cu:L = 1 : 2.

a)

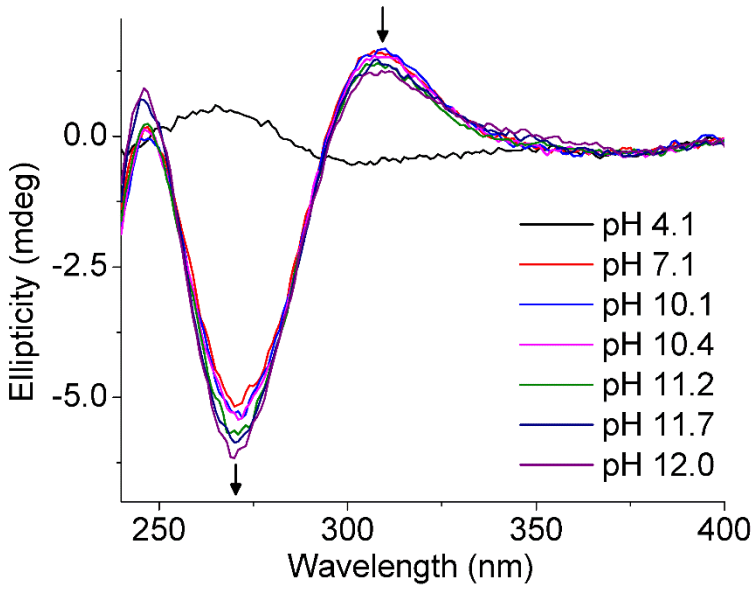

b)

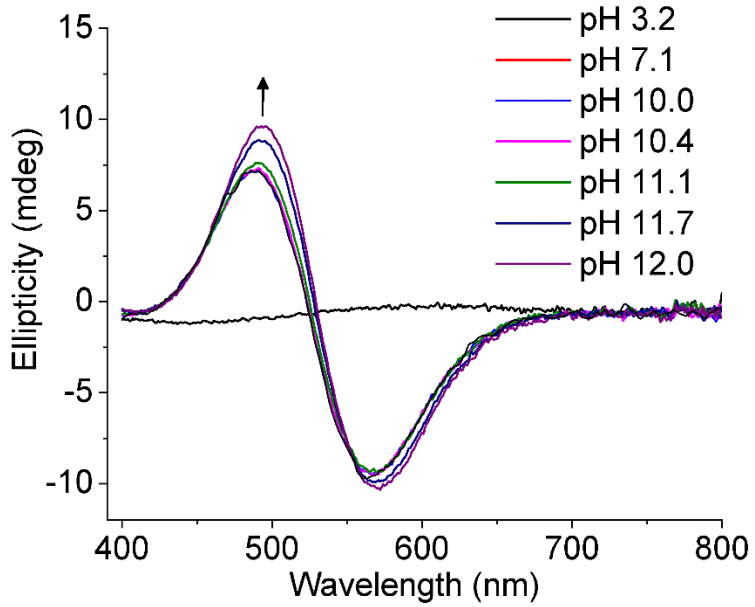

Fig. 6. Representative distribution diagrams for complex-formation of HAWG-NH_2 with Cu(II), at *T* = 25 °C and *I* = 0.1 M (KCl). C_{Cu} = 1 mM; a) Cu : L = 1 : 2; b) Cu : L = 1 : 1.

a)

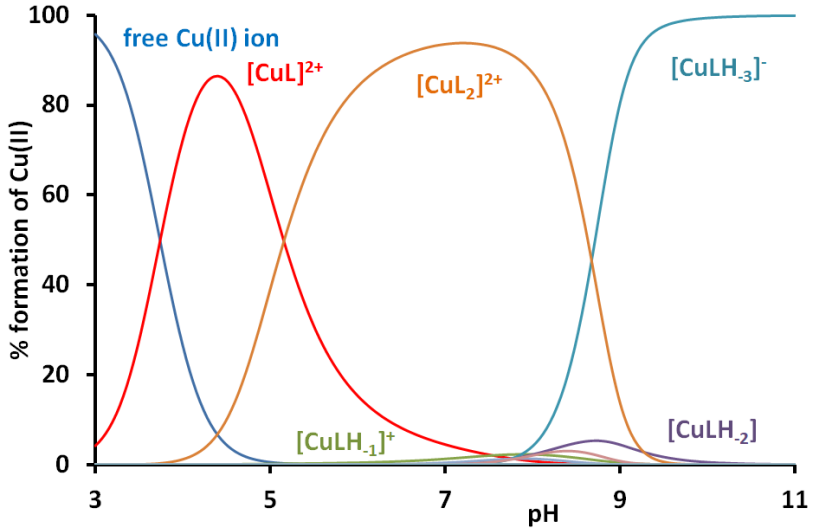

b)

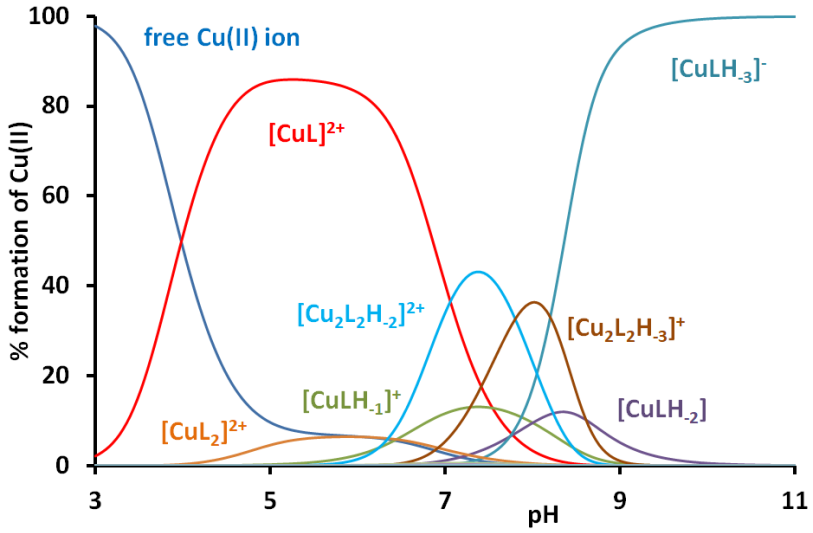

Fig. 7. Vis absorption spectra at variable pH for the binary solutions of HAWG-NH_2 with Cu(II), at T = 25 °C and I = 0.1 M (KCl). C_{Cu} = 0.556 mM; Cu / L = 1 : 2.2. Purple: pH 3.0; red: pH 4.5; orange: pH 7.1; cyan: pH 10.5.

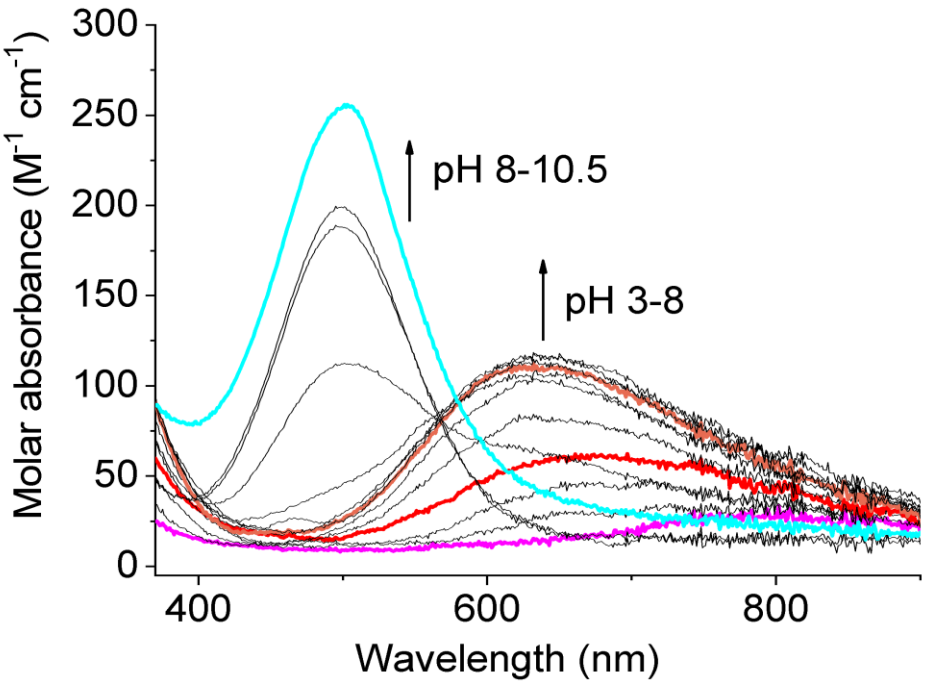

Fig. 8. a) UV and b) visible circular dichroism spectra at variable pH of a Cu(II) / HAWG-NH_2 solution, at *T* = 25 °C and *I* = 0.1 M (KCl). UV spectra: C_{Cu} = 50 µM; Vis spectra: C_{Cu} = 0.52 mM; Cu/L molar ratio = 1 : 2.

a)

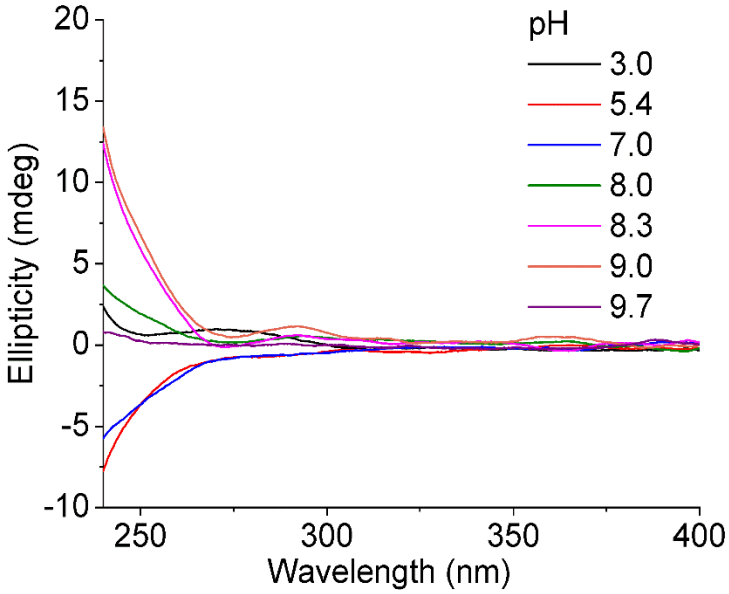

b)

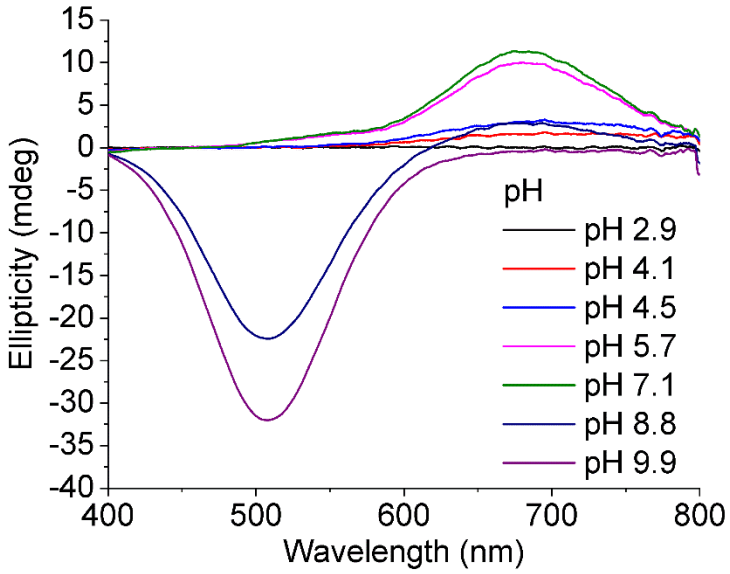

Fig. 9. Spectrophotometric titrations of HAWG-NH_2 with Cu(II) at pH 7.0 (a) and at pH 9.0 (b). C_L= 0.70 mM, aqueous HEPES or CHES buffer 25 mM for pH 7.0 and 9.0, respectively. Green dots represent absorbance values. Scale is reported on the right axes. Lines represent the speciation diagrams for the titration experiments (scale on the left axes).

a)

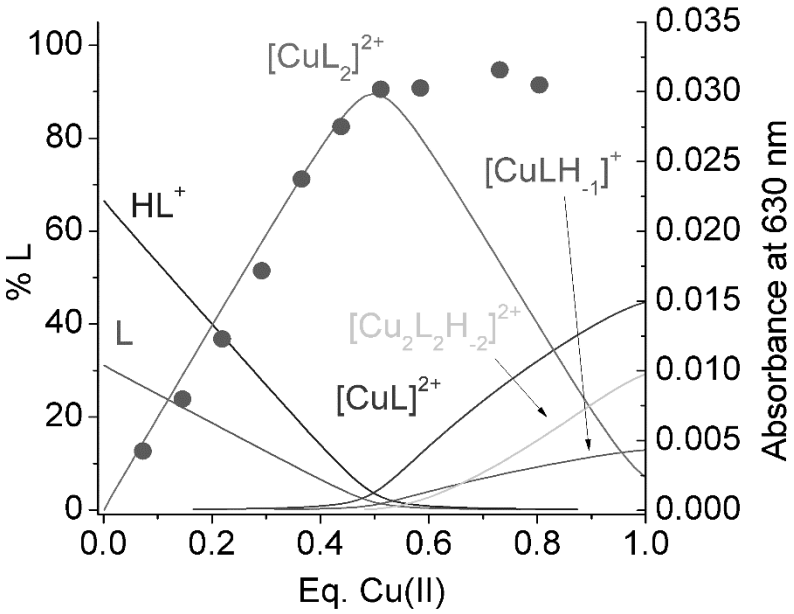

b)

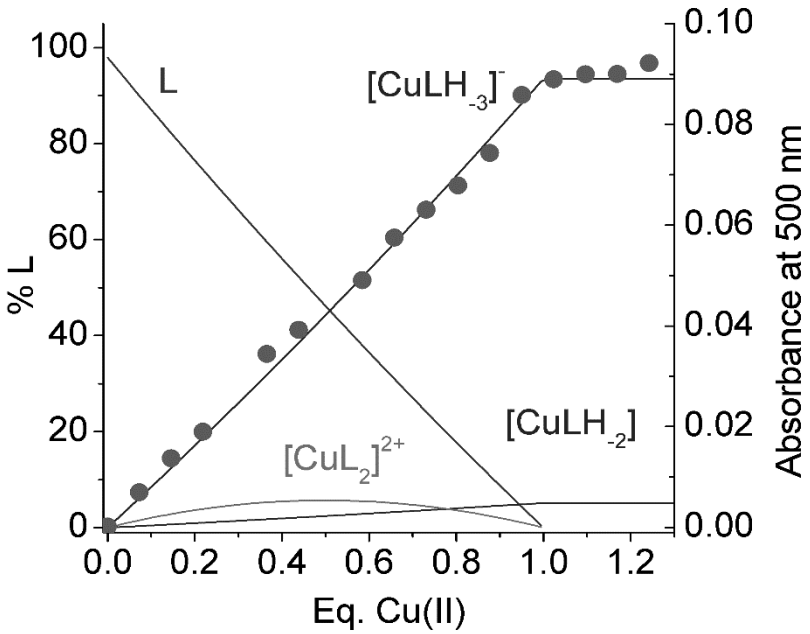

Fig. 10. Spectrofluorimetric titrations of HAWG-NH_2 with Cu(II) at pH 7.0 (a) and at pH 9.0 (b). C_L= 48 μM, aqueous HEPES or CHES buffer 25 mM for pH 7.0 and 9.0, respectively). Green dots represent emission values at 350 nm (λ_{exc}= 280 nm). Scale is reported on the right axes. Lines represent the speciation diagrams for the titration experiments (scale on the left axes).

a)

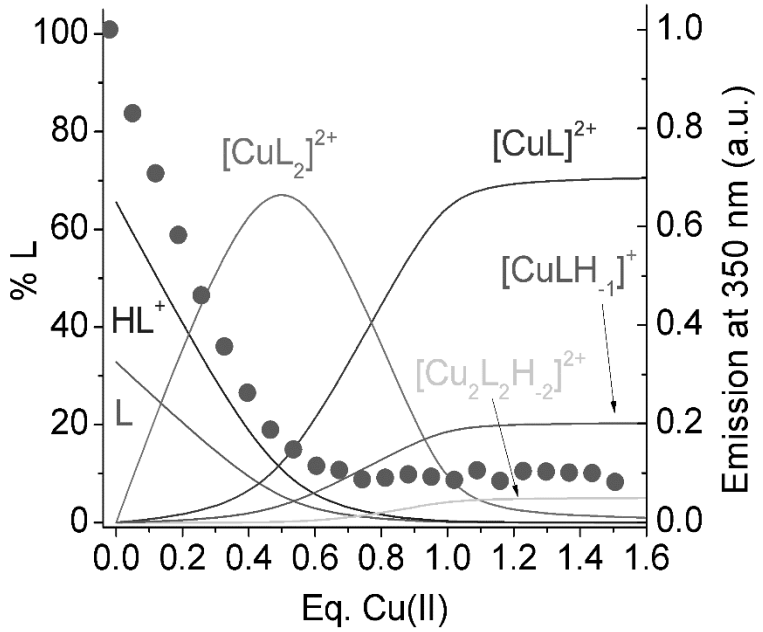

b)

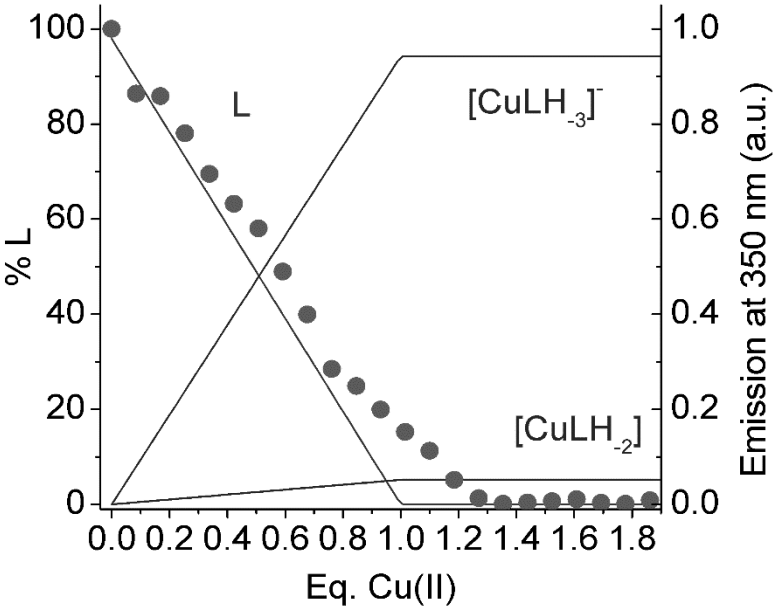

Fig. 11. a) Spectrophotometric (absorbance at 522 nm, C_L= 0.17 mM) and b) spectrofluorimetric (λ_{exc}= 280 nm; λ_{emis}= 350 nm, C_L= 48 µM) titrations for a solution of $(AAHAWG)_4$-**PWT2** with Cu(II) at pH 7.4 (aqueous HEPES buffer 25 mM).

a)

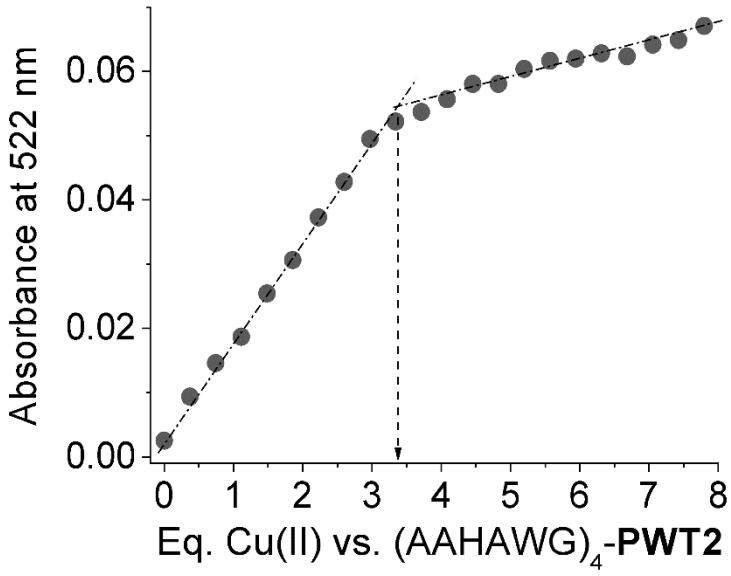

b)

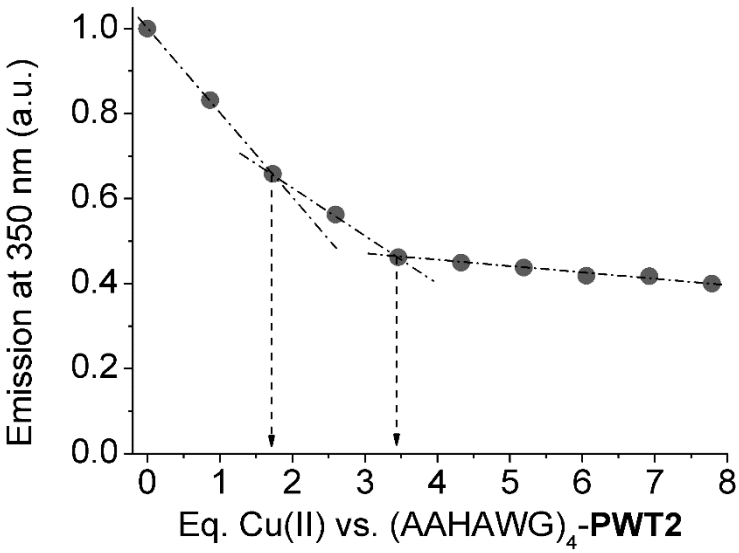

Fig. 12. Spectrofluorimetric titrations for a solution of $(HAWG)_4$-**PWT2** with Cu(II) at a) pH = 7.0 (HEPES buffer 25 mM) and b) pH = 9.0 (CHES buffer 25 mM). λ_{exc}= 280 nm; λ_{emis}= 350 nm, C_L= 48 µM.

a)

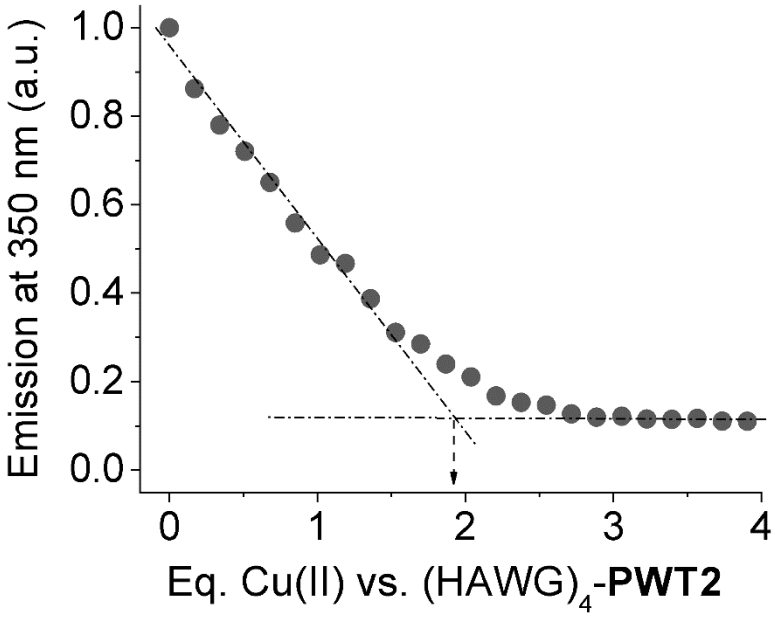

b)

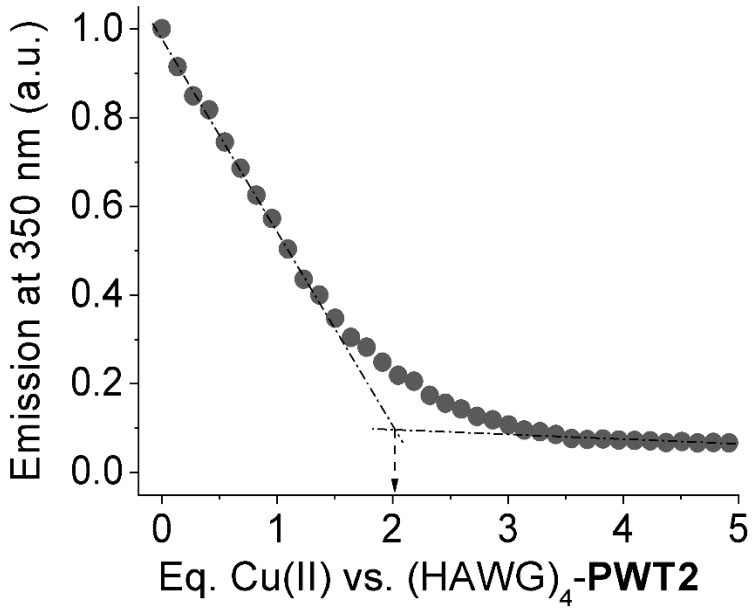

Fig. 13. Visible spectrophotometric titrations for a solution of $(HAWG)_4$-**PWT2** with Cu(II) at a) pH = 7.0 (HEPES buffer 25 mM) and b) pH = 9.0 (CHES buffer 25 mM). C_L= 0.20 mM. The spectra at highest Cu(II) content corresponds to 4 (pH 7.0) and 0.6 eq. (pH 9.0) of Cu(II) vs. ligand, respectively.

a)

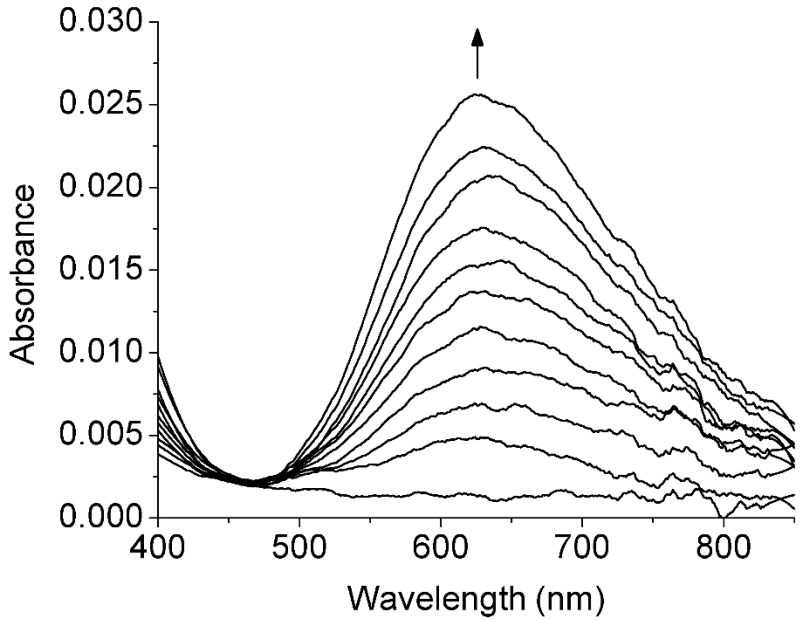

b)

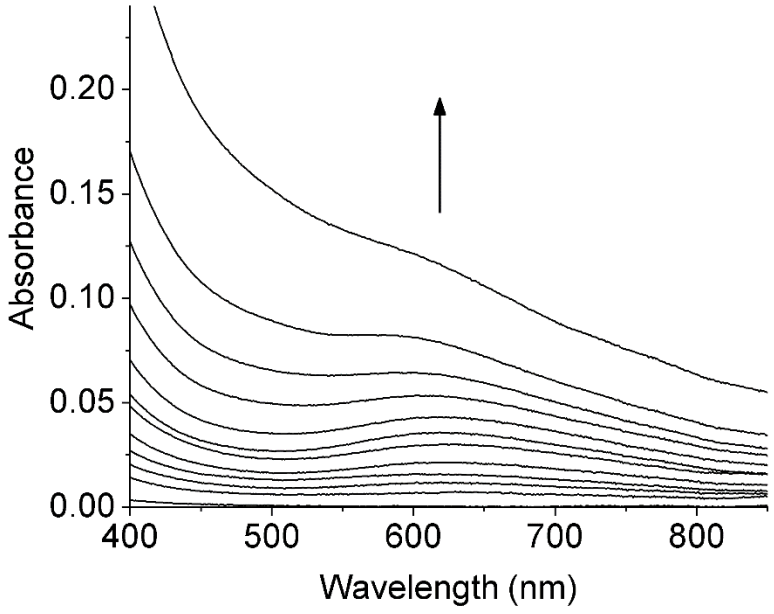

Fig. 14. Structural hypothesis for the complex [Cu(II)(AAHAWG-NH_2)H_{-2}]. Color code: orange=copper, blue=nitrogen, red=oxygen, light grey=hydrogen, grey=carbon.

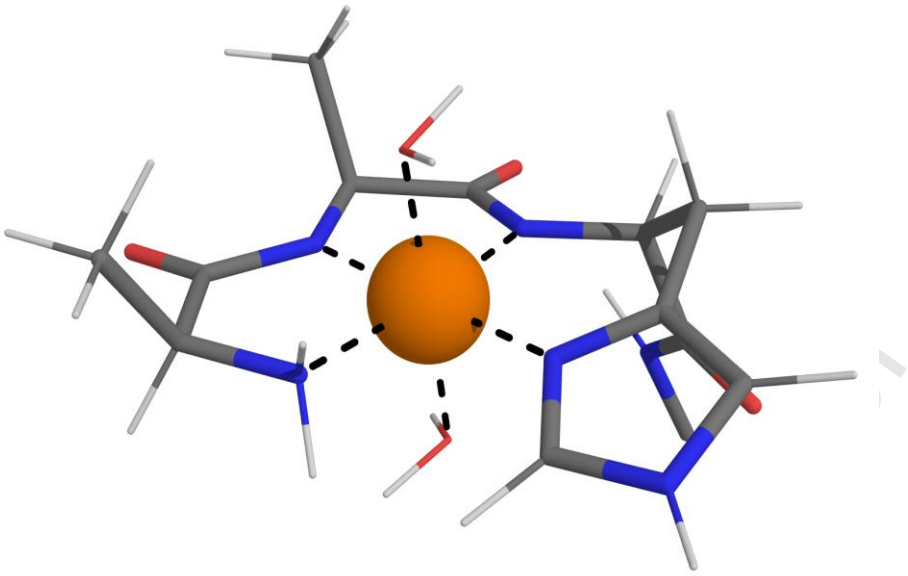

Fig. 15. Structural hypothesis for the complex $[Cu(II)(HAWG\text{-}NH_2)_2]^{2+}$. Color code: orange=copper, blue=nitrogen, red=oxygen, light grey=hydrogen, grey=carbon.

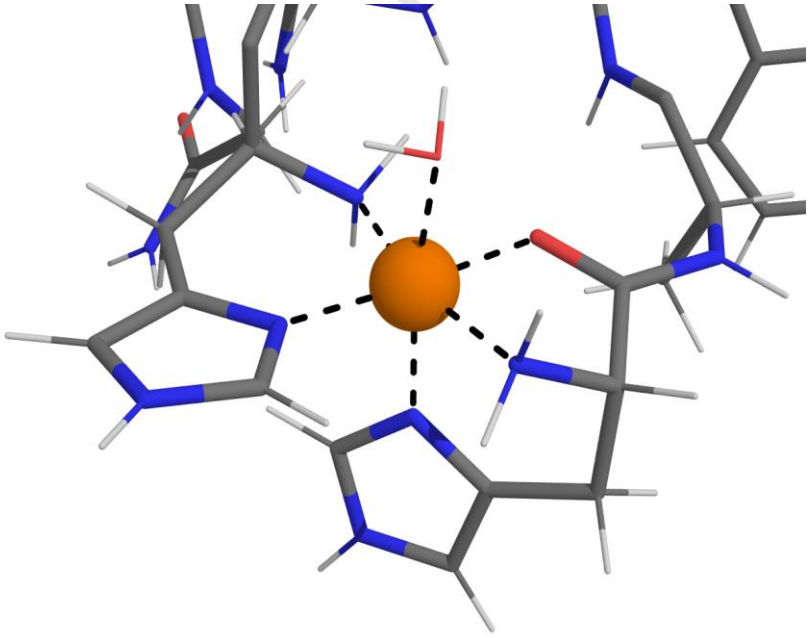

Fig. 16. Structural hypothesis for the complex [Cu(II)(HAWG-NH_2)H_{-3}]$^-$. Color code: orange=copper, blue=nitrogen, red=oxygen, light grey=hydrogen, grey=carbon.

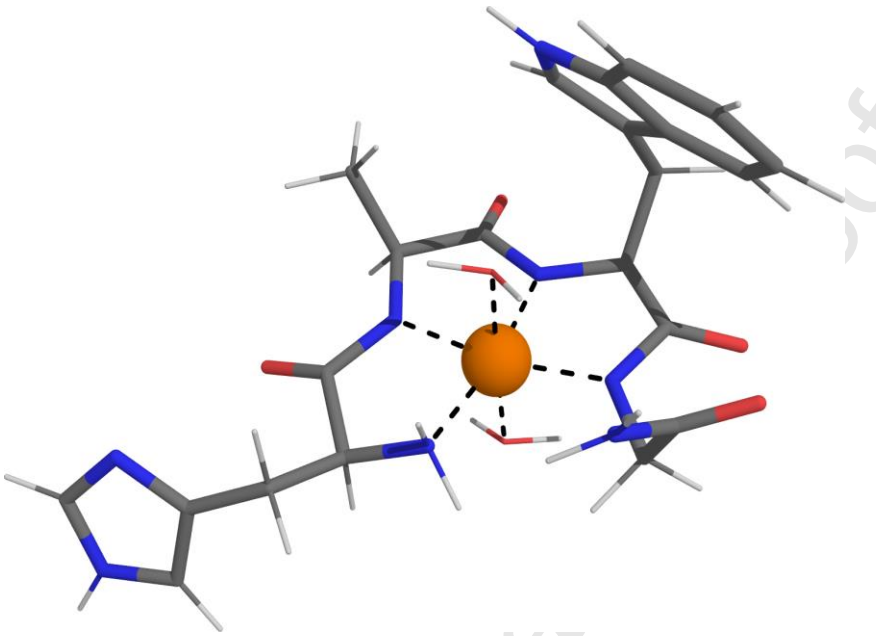

Declaration of competing interests

☒ The authors declare that they have no known competing financial interests or personal relationships that could have appeared to influence the work reported in this paper.

☐The authors declare the following financial interests/personal relationships which may be considered as potential competing interests:

Graphical abstract

Branched peptides can show metal binding properties different from those of the corresponding linear peptides, due to an exceptionally high local concentration of N-termini that act as binding sites.

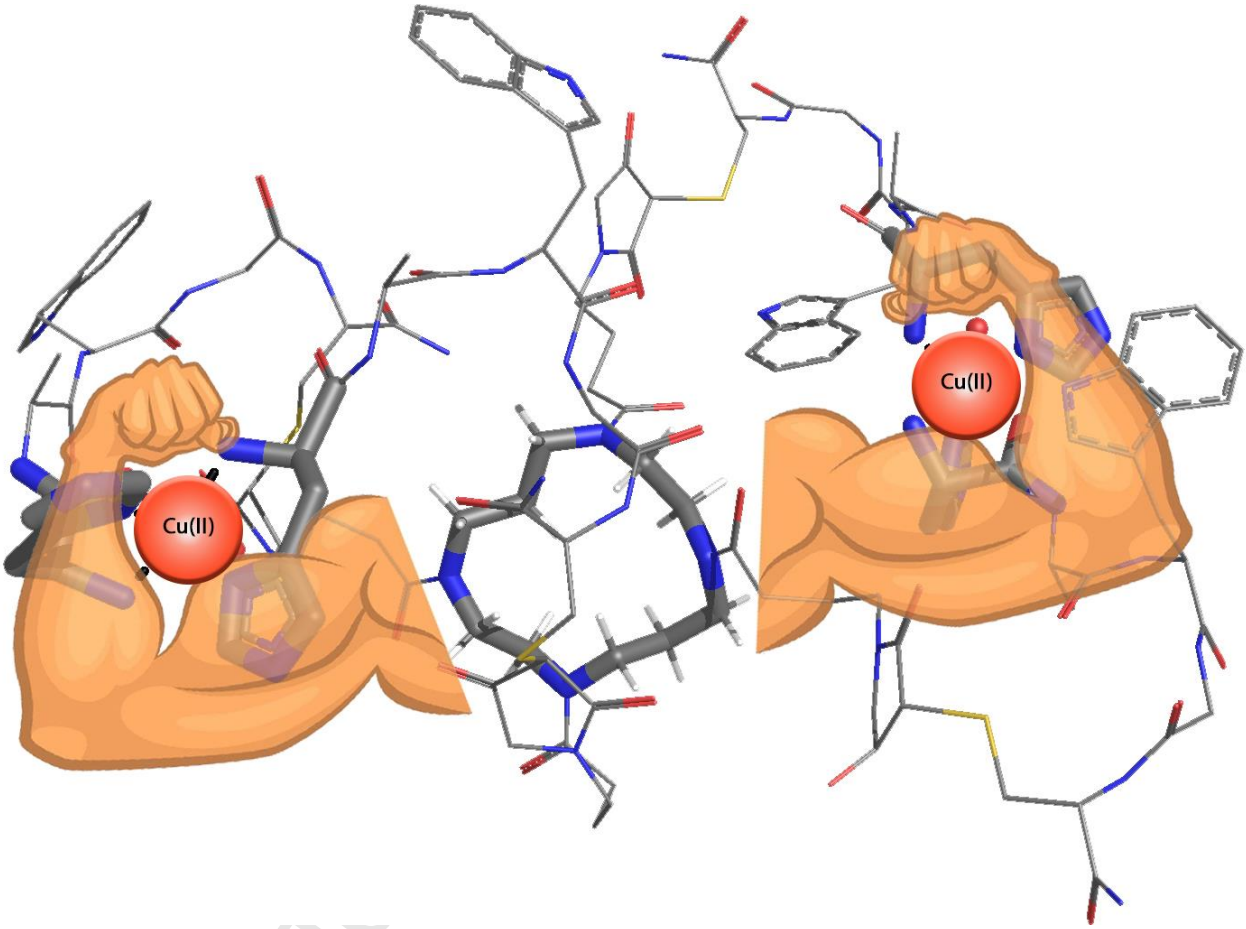

Highlights

A cyclam-based scaffold obtained by “peptide welding technology” (**PWT2**) was employed

The two branched peptides $(AAHAWG)_4$-PWT2 **and $(HAWG)_4$-**PWT2 **where synthesized**

Cu(II) complexes of branched and simple peptides were studies in aqueous solution

$(AAHAWG)_4$-PWT2 behaves as a Cu(II) chelator very similarly to AAHAWG-NH_2

$(HAWG)_4$-PWT2 showed a peculiar complexation mode at alkaline pH